Glucagon-like peptide-1 receptor signaling modifies the extent of diabetic kidney disease through dampening the receptor for advanced glycation end products–induced inflammation

OPEN

Karly C. Sourris[1,2,14], Yi Ding[2,3,14], Scott S. Maxwell[4], Annas Al-sharea[5], Phillip Kantharidis[1], Muthukumar Mohan[1], Carlos J. Rosado[1], Sally A. Penfold[2], Claus Haase[3], Yangsong Xu[5], Josephine M. Forbes[6], Simon Crawford[7], Georg Ramm[7], Brooke E. Harcourt[8], Karin Jandeleit-Dahm[1], Andrew Advani[9], Andrew J. Murphy[5], Daniel B. Timmermann[10], Anil Karihaloo[11], Lotte Bjerre Knudsen[10], Assam El-Osta[4], Daniel J. Drucker[12], Mark E. Cooper[1,15] and Melinda T. Coughlan[1,2,13,15]

[1]Department of Diabetes, Monash University, Central Clinical School, Alfred Research Alliance, Melbourne, Victoria, Australia; [2]Diabetes Complications Division, Baker Heart & Diabetes Institute, Melbourne, Victoria, Australia; [3]Diabetes Complications Research, Novo Nordisk, Måløv, Denmark; [4]Epigenetics in Human Health and Disease Program, Baker Heart & Diabetes Institute, Melbourne, Victoria, Australia; [5]Haematopoiesis and Leukocyte Biology, Division of Immunometabolism, Baker Heart & Diabetes Institute, Melbourne, Victoria, Australia; [6]Mater Research Institute, the University of Queensland, Translational Research Institute, Woolloongabba, Queensland, Australia; [7]Monash Ramaciotti Centre for Cryo Electron Microscopy, Monash University, Clayton, Victoria, Australia; [8]Murdoch Research Institute, Royal Children's Hospital, Melbourne, Victoria, Australia; [9]Keenan Research Centre for Biomedical Science and Li Ka Shing Knowledge Institute, St. Michaels Hospital, Toronto, Ontario, Canada; [10]Novo Nordisk, Copenhagen, Denmark; [11]Novo Nordisk Research Center Seattle, Inc., Seattle, Washington, USA; [12]Department of Medicine, Lunenfeld-Tanenbaum Research Institute, Mt. Sinai Hospital, University of Toronto, Toronto, Ontario, Canada; and [13]Drug Discovery Biology, Monash Institute of Pharmaceutical Sciences, Monash University Parkville Campus, Parkville, Victoria, Australia

Glucagon like peptide-1 (GLP-1) is a hormone produced and released by cells of the gastrointestinal tract following meal ingestion. GLP-1 receptor agonists (GLP-1RA) exhibit kidney-protective actions through poorly understood mechanisms. Here we interrogated whether the receptor for advanced glycation end products (RAGE) plays a role in mediating the actions of GLP-1 on inflammation and diabetic kidney disease. Mice with deletion of the GLP-1 receptor displayed an abnormal kidney phenotype that was accelerated by diabetes and improved with co-deletion of RAGE *in vivo*. Activation of the GLP-1 receptor pathway with liraglutide, an anti-diabetic treatment, downregulated kidney RAGE, reduced the expansion of bone marrow myeloid progenitors, promoted M2-like macrophage polarization and lessened markers of kidney damage in diabetic mice. Single cell transcriptomics revealed that liraglutide induced distinct transcriptional changes in kidney endothelial, proximal tubular, podocyte and macrophage cells, which were dominated by pathways involved in nutrient transport and utilization, redox sensing and the resolution of inflammation. The kidney-protective action of liraglutide was corroborated in a non-diabetic model of chronic kidney disease, the subtotal nephrectomised rat. Thus, our findings identify a novel glucose-independent kidney-protective action of GLP-1-based therapies in diabetic kidney disease and provide a valuable resource for exploring the cell-specific kidney transcriptional response ensuing from pharmacological GLP-1R agonism.

Kidney International (2023) ■, ■–■; https://doi.org/10.1016/j.kint.2023.09.029

KEYWORDS: diabetes; diabetic kidney disease; glucagon-like peptide-1; kidney; receptor for advanced glycation end products

Diabetic kidney disease (DKD) occurs in up to 40% of individuals with diabetes and remains the primary cause of kidney failure worldwide,[1–3] accounting for at least a third of all cases requiring renal replacement therapy.[4] The outlook for DKD has improved over recent decades as a result of improved blood glucose control, blood pressure management with an emphasis on renin-angiotensin system blockade, and, more recently, the use of sodium-glucose cotransporter-2 inhibitors. However, a significant proportion of individuals with diabetes will still progress to kidney failure or die prematurely from a cardiovascular event.[5–7]

Glucagon-like peptide-1 (GLP-1) is a gut-derived incretin hormone, which is produced and released by the L cells of the gastrointestinal tract after meal ingestion.[8] GLP-1 potentiates glucose-dependent insulin secretion from pancreatic islets via a single canonical receptor, the GLP-1R,[8,9] but increasingly,

Correspondence: *Karly C. Sourris or Melinda T. Coughlan, Department of Diabetes, Monash University, Melbourne, Victoria, Australia. E-mail: Karly.Sourris@monash.edu or melinda.coughlan@monash.edu*

[14]KCS and YD are equal first authors.

[15]MEC and MTC are equal last authors.

Received 15 February 2023; revised 16 September 2023; accepted 25 September 2023

Translational Statement

Considerable interest exists in identifying the actions of incretin-based therapies beyond glucose lowering, particularly in the kidney. In this study, we showed that mice with genetic disruption of *Glp1r* spontaneously develop chronic renal injury. We demonstrate that superimposition of diabetes in *Glpr1r*-deficient mice accelerated diabetic kidney disease (DKD) development and the phenotypic changes could be reversed by deletion of the proinflammatory receptor for advanced glycation end products (*Ager*). Treatment of diabetic mice with a glucagon-like peptide-1 receptor agonist (GLP-1RA), liraglutide, reduced kidney injury. Unbiased exploration using single-cell transcriptomics of kidney identified that GLP-1R agonism with liraglutide in diabetic mice remodeled a network of nutrient synthesis and transport, and promoted redox sensing signals in the proximal tubule, podocyte, and macrophage cell populations. Liraglutide treatment led to dampening of inflammatory signals in macrophages. This study demonstrates the importance of intact GLP-1R signaling in the maintenance of kidney homeostasis, provides a rationale for investigating GLP-1RA for the treatment of non-DKDs, and highlights the glucose-independent renal benefits of GLP-1RA.

extrapancreatic functions of GLP-1 are being reported. Both experimental[10,11] and more recently clinical studies such as the LEADER (Liraglutide Effect and Action in Diabetes: Evaluation of Cardiovascular Outcome Results)[12] and the REWIND (Researching Cardiovascular Events with a Weekly Incretin in Diabetes)[13] trials using GLP-1R agonists (GLP-1RA) such as liraglutide and dulaglutide, respectively, have demonstrated renoprotective actions of GLP-1 receptor agonism. However, whether these effects are glucose-independent has remained difficult to determine.

Receptor for advanced glycation end products (RAGE) is a multiligand, type 1 pattern recognition receptor and a member of the immunoglobulin superfamily that is central in mediating the proinflammatory actions of its ligands, including the danger-associated molecular patterns S100 proteins (calgranulins), AGEs, and high-mobility group box 1.[14–17] Although its basal expression is generally low, RAGE is expressed at high levels in the vascular endothelium and leukocytes and is induced in most cell types after injury, hypoxia, or inflammation, including in the kidney, in particular, the proximal tubular cells,[18] podocytes,[19] and mesangial cells.[20–22] Our group[23–25] and others[26,27] have demonstrated that the deletion of RAGE in mice confers renoprotection via dampening effects on oxidative stress and profibrotic pathways, whereas RAGE overexpression accelerates nephropathy in mouse models.[28] Results from *in vitro* studies have suggested that GLP-1 can modulate RAGE signaling and expression in multiple cell types.[29,30]

Considerable interest exists in identifying the actions of incretin-based therapies beyond glucose lowering, and a direct action of GLP-1 on the kidney has been proposed.[31,32] Although GLP-1R has been shown to be expressed within the kidney at low levels,[33–36] the role of GLP-1 signaling in the kidney is still undefined. The present study aimed to address the gap in our understanding of GLP-1 action in DKD by exploring the interaction between GLP-1 and RAGE in the kidney, in settings where glucose-lowering effects of GLP-1R agonism are absent, such as (i) loss of function studies in animal models with the absence of a functional GLP-1R, (ii) gain of function signaling through the GLP-1R pathway using a GLP-1 analog in animals with or without diabetes, and (iii) unbiased molecular network analysis using single-cell transcriptomics to assess kidney cell–specific changes in response to pharmacologic GLP-1R signaling.

METHODS

For detailed methods, refer to Supplementary Methods. The ARRIVE (Animal Research: Reporting of In Vivo Experiments) guidelines 2.0 for experimental design and reporting animal research were followed.[37]

Animal studies

Generation of RAGE x GLP-1R double knockout mice. Mice deficient in either *Ager*, *Glpr1*, or both *Ager* and *Glpr1* (*Ager-Glp1r*$^{-/-/-/-}$ double knockout [dKO]) were generated on a C57BL/6J background (wild-type) (WT; C57BL/6J). *Ager*$^{-/-}$ mice were kindly donated by Prof. Angelika Bierhaus, University of Heidelberg, Germany.[38,39] *Glp1r*$^{-/-}$ mice were kindly donated by Prof. Daniel Drucker, University of Toronto, Canada.[40] To generate the dKO mice, *Ager*$^{-/-}$ mice were crossed with *Glp1r*$^{-/-}$ KO mice. The resulting *Ager-Glp1r*$^{+-/+-}$ heterozygous mice were crossed and, after 4 generations, the *Ager-Glp1r*$^{-/-/-/-}$ mouse was generated, and a colony was established from these founders. The colony was maintained as *Ager-Glp1r*$^{+-/+-}$ heterozygous mice in order to obtain WT littermates. For details of chemical-induced diabetes and study protocol, refer to Supplementary Methods.

Ins2^{Akita} mice. Diabetic Ins2^{Akita} mice (C57BL/6-*Ins2^{Akita}*/J) and their WT counterparts were purchased from the Jackson Laboratory (Strain #003548), and at 6 weeks of age, male WT or heterozygous Ins2^{Akita} mice were randomly assigned to receive either vehicle (phosphate-buffered saline/Tween 80) or liraglutide (Lira, 50 μg/kg) by daily subcutaneous injection for 20 weeks (n = 12 mice per group), or the angiotensin-converting enzyme inhibitor (ACEi) perindopril (2 mg/kg) provided in the drinking water. A separate group of heterozygous Ins2^{Akita} mice were administered a combination therapy consisting of liraglutide and perindopril (L+A) for 20 weeks (n = 12 mice per group).

Rat subtotal nephrectomy model. Female Fischer 344 rats (Charles River) aged 8 weeks were randomized to undergo subtotal nephrectomy (SNx) or sham surgery, as previously described.[41] Briefly, animals were anesthetized with 2.5% isoflurane, the right kidney was removed via subcapsular nephrectomy, and infarction of approximately two-thirds of the left kidney was achieved via selective ligation of 2 of the 3 or 4 branches of the left renal artery. Sham surgery consisted of laparotomy and manipulation of both kidneys before wound closure. One week after surgery, rats were randomized to receive liraglutide (Novo Nordisk Canada Inc.) 0.2 mg/kg twice daily subcutaneously[42] or phosphate-buffered saline (n = 6–12 per group) for 7 weeks.

Statistical analysis

Data are expressed as means ± SD, unless otherwise stated. The analyses of experimental data were performed by either 1-way or 2-way

analysis of variance followed by *post hoc* analysis using the Tukey test or unpaired Student *t* tests. Outliers were identified and excluded using the ROUT (Robust Regression Outlier Removal) test. Data for albuminuria were not normally distributed and therefore analyzed after logarithmic transformation. The level of statistical significance was set *a priori* at $P < 0.05$. GraphPad Prism (version 9.3.1) was used for all statistical analyses.

RESULTS

Loss of GLP-1R drives a renal phenotype that is accelerated by diabetes

GLP-1-based therapies are thought to directly influence renal physiology and have indirect metabolic and hemodynamic actions that might reduce renal risk in diabetes; however, GLP-1 action on the kidney is not well understood.[31] Accordingly, to explore the physiological involvement of the GLP-1R signaling pathway in the regulation of kidney function, we studied mice with global genetic deletion of the receptor *Glp1r* (*Glpr1r*$^{-/-}$ mice) and their WT littermates (C57BL/6 background) (Figure 1a). After 24 weeks of observation, *Glp1r*$^{-/-}$ mice spontaneously developed kidney injury as shown by albuminuria (Figure 1b), a reduction in plasma cystatin C (Figure 1c), an increase in cortical fibronectin deposition (Figure 1d), and glomerulosclerosis (Figure 1e and f).

We next assessed the susceptibility of mice with GLP-1R deficiency and experimental diabetes to the development of DKD by injecting *Glpr1r*$^{-/-}$ mice with streptozotocin (STZ) to induce insulin deficiency resembling type 1–like diabetes. *Glpr1r*$^{-/-}$ mice injected with STZ exhibited worsened albuminuria compared with either *Glpr1r*$^{-/-}$ mice in the absence of STZ or WT STZ-treated mice (Figure 1b). Together, these data highlight the importance of an intact GLP-1 signaling pathway in maintaining kidney health.

Genetic deletion of RAGE in *Glp1r*$^{-/-}$ mice improves diabetes-associated kidney injury

Our group[23–25] and others[26,27] have demonstrated that the deletion of RAGE confers a protective effect on kidney function, and previous *in vitro* work has suggested that GLP-1 can interfere with RAGE signaling.[29,30] To ascertain whether the loss of RAGE attenuates renal injury in the absence of the GLP-1R, we deleted RAGE in *Glpr1r*-deficient mice by cross-breeding *Ager*$^{-/-}$ mice with *Glpr1r*$^{-/-}$ mice to produce *Ager*$^{-/-}$:*Glp1r*$^{-/-}$ dKO mice and studied these mice in the presence or absence of STZ-induced diabetes for 24 weeks (Figure 2a). The deletion of RAGE protein in the kidneys of the *Ager*$^{-/-}$ mouse and the dKO mouse was confirmed by the enzyme-linked immunosorbent assay of plasma membrane–enriched extracts of the kidney cortex (Figure 2b). The absence of GLP-1R in the *Glpr1r*$^{-/-}$ single and dKO mice was confirmed by quantitative polymerase chain reaction of the kidney cortex (Figure 2c). Primer sequences are reported in Supplementary Table S1.

After 24 weeks, STZ diabetic mice displayed reduced body weight (Supplementary Figure S1A), increased food intake (Supplementary Figure S1B), increased blood glucose (Supplementary Figure S1C), and glycated hemoglobin (Supplementary Figure S1D), which was consistent across genotypes. Water intake (Supplementary Figure S1E) and urine output (Supplementary Figure S1F) were similarly increased in all diabetic mice and were not differentially affected in the KO mice. These data indicate that the deletion of either *Ager*, *Glp1r*, or both *Ager* and *Glp1r* simultaneously does not alter glycemic control nor feeding behaviors in mice with STZ-induced diabetes, indicating that the renal phenotypes observed were independent of differences in metabolic control.

RAGE protein was upregulated in the kidneys of normoglycemic *Glpr1r*$^{-/-}$ mice (Figure 2b). In the setting of STZ diabetes, RAGE protein was further upregulated in STZ-treated WT and *Glpr1r*$^{-/-}$ mice (Figure 2b). In WT diabetic mice, *Glp1r* mRNA expression was downregulated in the kidney compared with nondiabetic controls (Figure 2c), yet a reduction of *Glp1r* mRNA expression was not observed in *Ager*$^{-/-}$ diabetic mice. Consistent with previous observations from our laboratory[23–25] and others,[26,27] the extent of albuminuria was reduced in *Ager*$^{-/-}$ mice with diabetes (Figure 2d). In contrast, *Glp1r*$^{-/-}$ mice with STZ diabetes exhibited increased albuminuria (Figure 2d). Deleting *Ager* and *Glp1r* in mice (dKO) attenuated albuminuria in the setting of diabetes (Figure 2d), indicating that RAGE is essential for increased albumin excretion rate in *Glp1r*$^{-/-}$ mice. Further investigation of the renal phenotype revealed a significant effect of diabetes status on plasma cystatin C, with a reduction in WT diabetic mice, which was not influenced by the deletion of *Ager* or *Glp1r* (Figure 2e). The glomerular sclerotic index histology score, although increased in WT diabetic mice and *Glp1r*$^{-/-}$ mice, was not increased in *Ager*$^{-/-}$ mice or dKO mice (Figure 2f and g). *Ager*$^{-/-}$ mice with diabetes had lower glomerular sclerotic index scores than WT diabetic mice, indicating a protective effect of *Ager* deletion on glomerulosclerosis (Figure 2f). The deletion of *Ager* may primarily act on structural rather than functional parameters with an effect on alleviating glomerular injury; the effect on albumin is presumed to be related to the amelioration of diabetes-associated podocyte injury.

The presence of kidney injury molecule (KIM)-1 in the urine is consistent with proximal tubular injury.[43] WT diabetic mice exhibited an increase in urinary KIM-1, and this was also seen in diabetic *Glp1r*$^{-/-}$ mice (Figure 2h). However, the deletion of *Ager* ameliorated the diabetes-induced excretion of KIM-1 (Figure 2h). Deleting both *Ager* and *Glp1r* (dKO) significantly reduced urinary KIM-1 in the context of diabetes. In addition, diabetes induced an increase in renal fibronectin expression in WT mice (Figure 2i). The deletion of *Ager* but not *Glp1r* decreased diabetes-induced fibronectin deposition. In the dKO mouse, fibronectin was reduced (Figure 2i), which is comparable to that seen in the RAGE KO mouse. Taken together, these data identify a role for GLP-1R deficiency in conferring susceptibility to kidney injury and worsening DKD outcome in an experimental model of diabetes.

GLP-1R belongs to the B family subclass of G protein–coupled receptors. GLP-1R preferentially couples to $G\alpha_S$-regulated pathways, favoring the production of cyclic adenosine

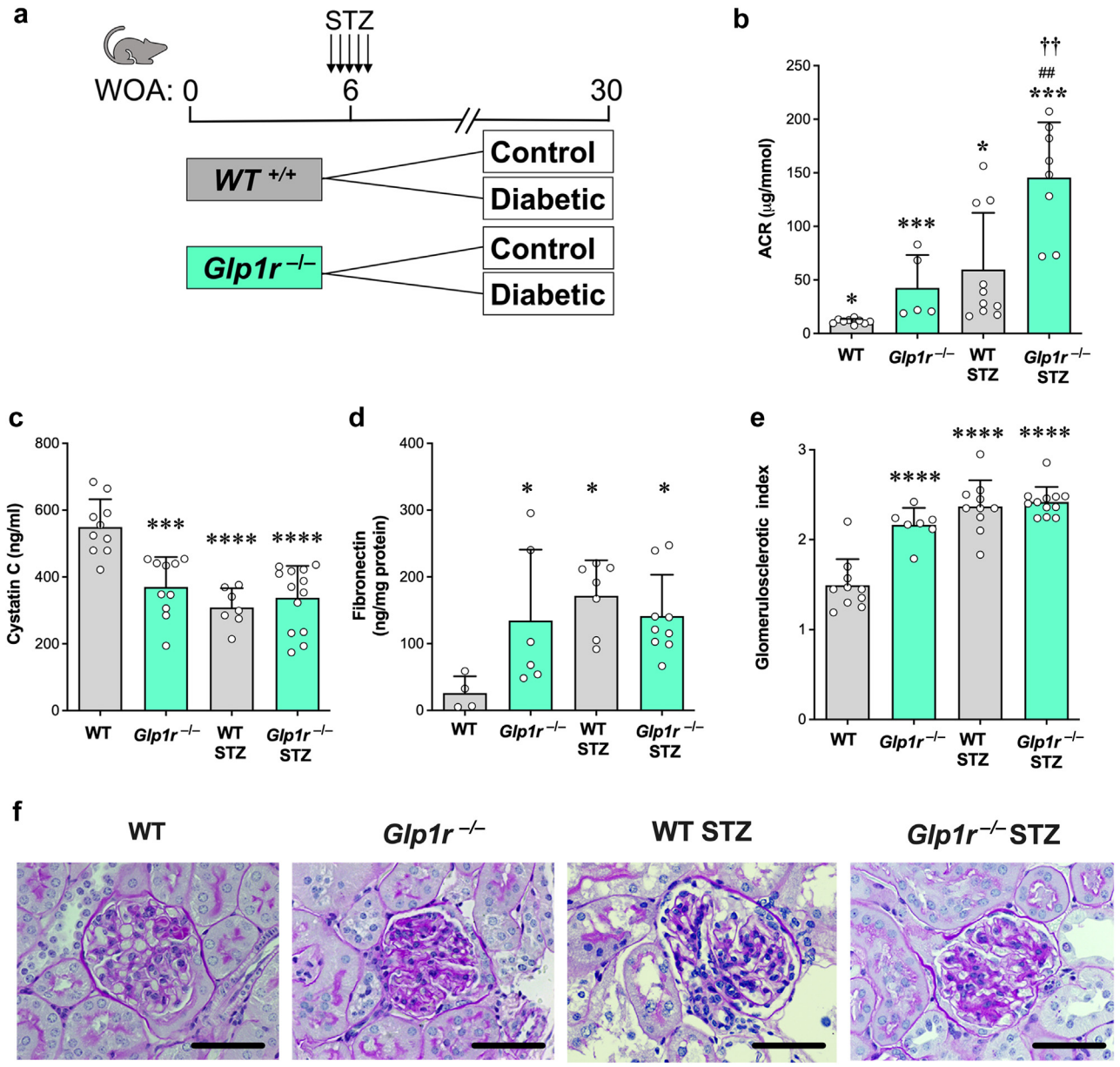

Figure 1 | Glucagon-like peptide-1 receptor (GLP-1R) deficiency is a susceptibility factor for nephropathy contributing to worsened diabetic kidney disease. (**a**) Schematic depicting the streptozotocin (STZ)-induced diabetes paradigm in wild-type (WT) and *Glp1r*$^{-/-}$ mice. After diabetes induction, mice were followed for 24 weeks. (**b**) Urinary albumin-to-creatinine (ACR) ratio and (**c**) plasma cystatin C. (**d**) Fibronectin in the kidney cortex. (**e**) Glomerular sclerotic index was quantitated using periodic acid–Schiff (PAS) staining and light microscopy under original magnification of ×400. (**f**) Representative PAS-stained kidney sections. Original magnification ×400 and Bar = 25 μm. Data are presented as mean ± SD (n = 5–10 per group). Dots represent individual mice. *P* values were determined by 2-way analysis of variance with the Tukey multiple comparison test. **P* < 0.05 versus WT, ****P* < 0.001 versus WT, *****P* < 0.0001 versus WT, ##*P* < 0.01 versus *Glp1r*$^{-/-}$, ††*P* < 0.01 versus WT STZ. *Glp1r*$^{-/-}$, *Glp1r* knockout mice; WOA, week of age. To optimize viewing of this image, please see the online version of this article at www.kidney-international.org.

monophosphate through increasing adenylate cyclase activity[44] and promoting the activation of signaling pathways coupled to protein kinase A (PKA). To establish that the decline in GLP-1R in the kidney in diabetes (WT mice) resulted in a decrease in GLP-1R canonical signaling, PKA activity was determined. Indeed, the decline in GLP-1R within the WT diabetic kidney was associated with a concomitant decrease in PKA activity compared with WT control (Supplementary Figure S2A). Moreover, RAGE-null mice with diabetes exhibited no change in kidney PKA activity compared with WT control or RAGE-null nondiabetic controls. Normoglycemic control mice with a deletion in *Glp1r* also exhibited reduced PKA activity. dKO mice did not have altered PKA activity in the diabetic setting (Supplementary Figure S2A). To assess pathophysiological

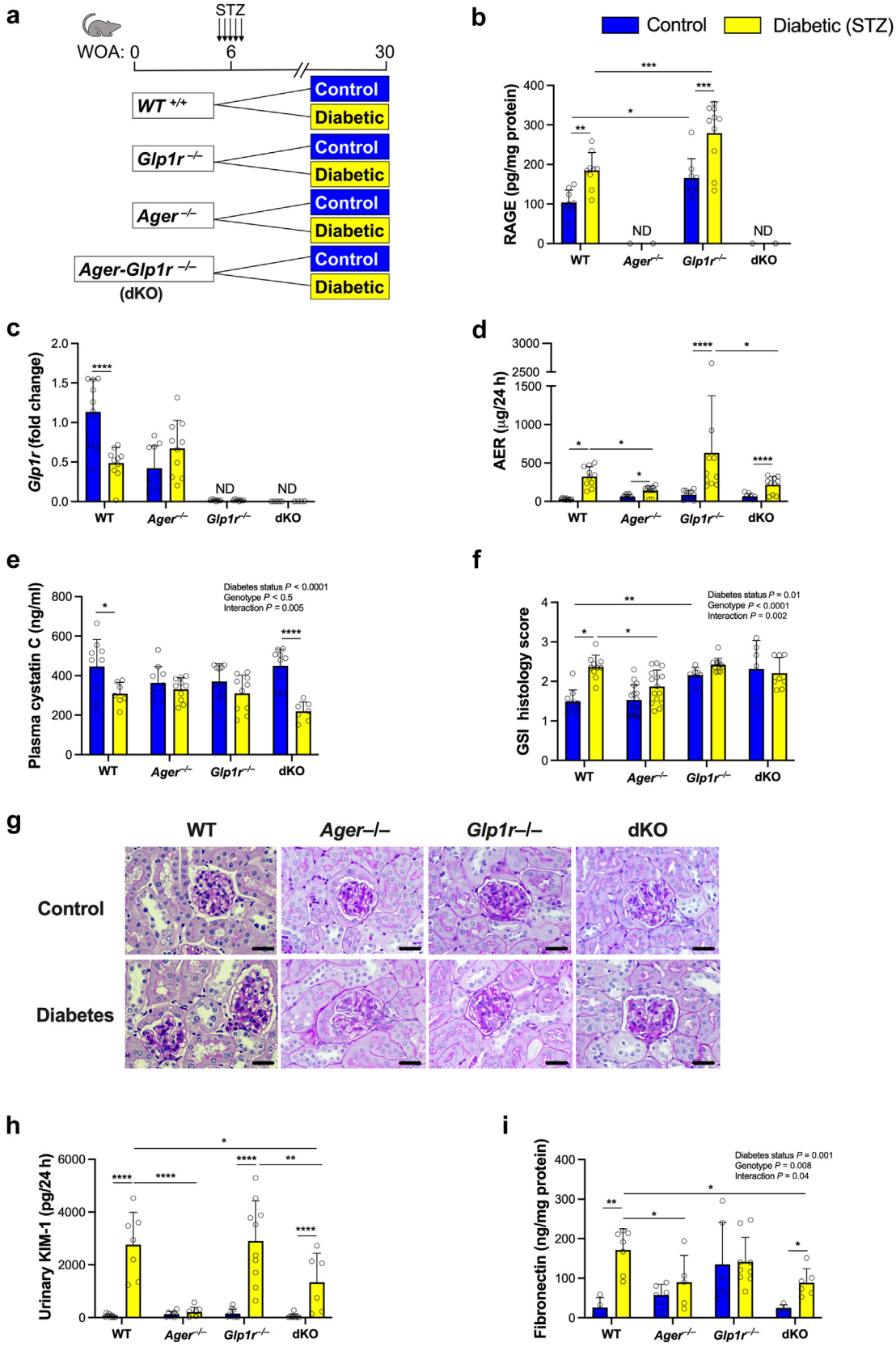

Figure 2 | Deletion of receptor for advanced glycation end products (RAGE) (*Ager*) in *Glp1r*$^{-/-}$ mice (*Ager-Glp1r*$^{-/-/-/-}$ mice) reverses key phenotypic changes in the setting of diabetic kidney disease. Wild-type (WT), *Glp1r*$^{-/-}$ mice, *Ager*$^{-/-}$ mice, and *Ager-Glp1r*$^{-/-/-/-}$ mice (dKO) with or without streptozotocin (STZ)-induced diabetes were followed for 24 weeks. (**a**) Schematic (continued)

pathways typically observed in DKD, we measured the levels of a marker of oxidative stress. Isoprostanes are prostaglandin-like compounds that are produced by free radical-mediated peroxidation of lipoproteins. Mice with diabetes had enhanced oxidative stress as reflected by an increase in urinary excretion of 15-isoprostane F_{2t}, which was dampened in response to the deletion of RAGE (Supplementary Figure S2B). Although *Glp1r*$^{-/-}$ mice did not display protection against diabetes-induced oxidative stress, urinary levels of 15-isoprostane F_{2t} were attenuated by co-deletion of *Ager* and *Glp1r* (dKO) (Supplementary Figure S2B). These data support the importance of RAGE in the development of kidney injury in *Glp1r*$^{-/-}$ mice.

The GLP-1R agonist liraglutide reverts podocyte injury and DKD

With our findings suggesting that GLP-1R deficiency exacerbates kidney injury in DKD, we next examined the actions of the clinically used GLP-1RA liraglutide in the insulin-2 *Akita* (*Ins2*^{Akita}) mouse. These animals develop pancreatic β-cell failure as a result of β-cell–selective proteotoxicity resulting from misfolding of insulin2 (*Ins2*)[45] and are a model of severe insulin deficiency suitable for the analysis of DKD.[46] Because the blockade of the renin-angiotensin system is the gold standard approach to slow the progression of DKD in subjects with diabetes, the ACEi perindopril was used alone, or in combination with liraglutide (L + A). Mice were treated from 6 weeks of age and followed for 20 weeks (Figure 3a). At the end of the study, blood glucose (Supplementary Figure S3A), glycated hemoglobin (Supplementary Figure S3B), food intake (Supplementary Figure S3C), water intake (Supplementary Figure S3D), and urinary output (Supplementary Figure S3E) were increased and body weight was reduced (Supplementary Figure S3F) in diabetic Ins2^{Akita} mice relative to WT controls. The administration of liraglutide (Lira), the ACEi perindopril, or coadministration of both liraglutide and perindopril (L + P) did not alter any of these parameters (Supplementary Figure S3A–F).

Ins2^{Akita} mice exhibited an increase in albuminuria relative to the WT littermate controls (Figure 3b). After 20 weeks of treatment, albuminuria was reduced with liraglutide or perindopril or their combination (Figure 3b). Ins2^{Akita} mice had a decrease in plasma cystatin C, and this was unaltered by liraglutide or perindopril alone or together (Figure 3c). Glomerulosclerosis was evident in Ins2^{Akita} mice and was reduced in liraglutide- but not perindopril-treated mice (Figure 3d and e). Transmission electron microscopy was performed in a subset of kidneys from control, diabetic, and diabetic mice treated with liraglutide. Image analysis of the glomerular basement membrane (GBM) demonstrated that GBM thickening was evident in the diabetic mice and that this GBM thickening was reversed with administration of liraglutide (Figure 3f and g). Liraglutide also restored the number of foot processes in podocytes per length of GBM in Ins2^{Akita} mice (Figure 3h), but it did not improve markers of tubular injury (urinary KIM-1) as was seen with the ACEi (Figure 3i). Furthermore, consistent with a liraglutide-mediated reduction in kidney fibrosis, levels of active transforming growth factor-β1 protein expression (Figure 3j), and glomerular fibronectin deposition, as measured by immunohistochemistry, were reduced in the renal cortex of liraglutide-treated mice (Figure 3k and l), emphasizing the protective role of GLP-1R agonism against podocyte injury and DKD.

Vehicle-treated Ins2^{Akita} mice showed reduced *Glp1r* expression (Supplementary Figure S4A) and PKA activity (Supplementary Figure S4B) in the kidney cortex compared with WT control mice. In Ins2^{Akita} mice, liraglutide partially restored *Glp1r* expression (Supplementary Figure S4A) and reversed the decrease in PKA activity (Supplementary Figure S4B). Vehicle-treated Ins2^{Akita} mice showed the upregulation of *Ager* expression (Supplementary Figure S4C) and RAGE protein (Supplementary Figure S4D) in the kidney cortex compared with WT control mice. In contrast, liraglutide downregulated kidney *Ager* expression (Supplementary Figure S4C) and RAGE protein (Supplementary Figure S4D) in Ins2^{Akita} mice, providing further evidence linking GLP-1R signaling to attenuation of RAGE activity.

Liraglutide attenuates diabetes-induced myelopoiesis and promotes the resolution of kidney inflammation

Because previous studies have shown that hyperglycemia associated with diabetes promotes enhanced myelopoiesis via RAGE and its ligands[47] and emerging evidence indicates that GLP-1-based therapies exhibit anti-inflammatory properties,[48,49] we explored key signals involved in "sterile" inflammation in Ins2^{Akita} mice treated with liraglutide. Canonical pathway activation of the pivotal mediator of inflammation, nuclear factor κB (p65), in the diabetic kidney was suppressed by liraglutide and perindopril (Figure 4a). Dysregulated innate immune responses mediated by macrophages are commonly observed in progressive renal injury.[50] Monocyte chemoattractant protein (MCP)-1 (also known as CC chemokine ligand 2) triggered upon exposure to inflammatory stimuli drives the chemotaxis of myeloid and lymphoid cells, regulating migration and infiltration of

Figure 2 | (continued) depicting the diabetes STZ paradigm in the various mouse genotypes. (**b**) Protein expression of RAGE was determined by the enzyme-linked immunosorbent assay (ELISA). (**c**) *Glp1r* mRNA expression was determined by quantitative polymerase chain reaction in the kidney cortex. (**d**) Urinary albumin excretion rate (AER) as determined by the ELISA in 24-hour urine collections. (**e**) Plasma cystatin C was measured by the ELISA. (**f**) Glomerular sclerotic index (GSI) histology score. GSI was quantitated using periodic acid–Schiff staining and light microscopy under original magnification of ×400. (**g**) Representative GSI images. Original magnification ×400 and Bar = 20 μm. (**h**) Urinary KIM-1 as determined by the ELISA in 24-hour urine collections. (**i**) Fibronectin in the kidney cortex. Data are presented as mean ± SD (n = 5–10 per group). Dots represent individual mice. *P* values were determined by 2-way analysis of variance with the Tukey multiple comparison test. *$P < 0.05$, **$P < 0.01$, ***$P < 0.001$, ****$P < 0.0001$. dKO, double knockout; *Glp1r*$^{-/-}$, *Glp1r* knockout mice; KIM, kidney injury molecule; ND, not detectable; WOA, week of age. To optimize viewing of this image, please see the online version of this article at www.kidney-international.org.

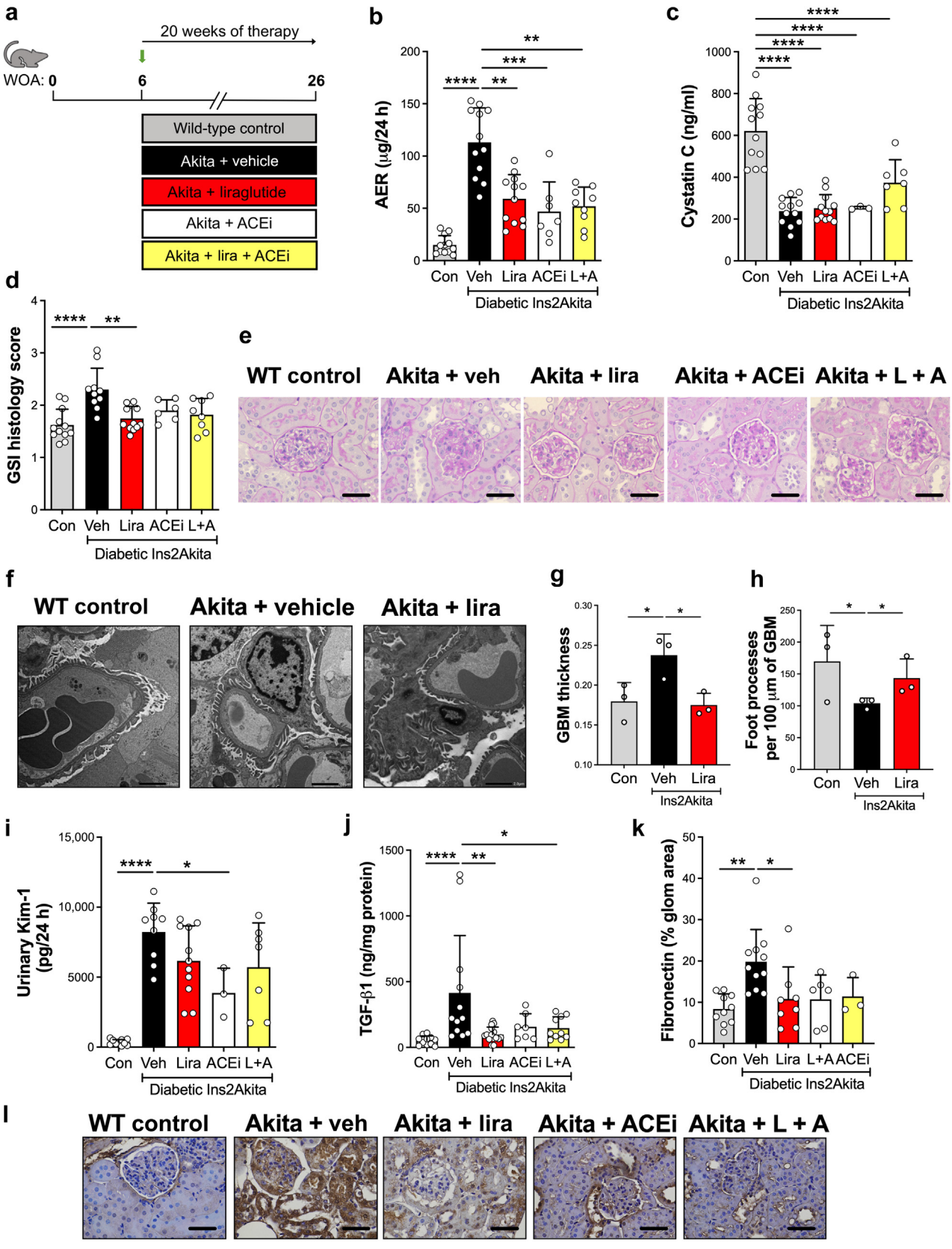

Figure 3 | Treatment with the glucagon-like peptide-1 receptor (GLP-1) receptor agonist liraglutide ameliorates podocyte injury and diabetic kidney disease. Ins2^{Akita} mice were treated with liraglutide, the angiotensin-converting enzyme inhibitor (ACEi) perindopril, or a combination of liraglutide and perindopril for 20 weeks. (**a**) Schematic depicting the treatment regimen. (**b**) Urinary albumin excretion rate (AER) as determined by the enzyme-linked immunosorbent assay (ELISA) in 24-hour urine collections. (**c**) Plasma cystatin C was (continued)

monocytes/macrophages to the sites of inflammation produced by tissue injury.[51] Indeed, MCP-1 protein expression was upregulated in the kidney cortex in vehicle-treated Ins2^{Akita} mice (Figure 4b). Both liraglutide and perindopril suppressed MCP-1 protein expression to a similar extent (Figure 4b). Interleukin-10 is a potent anti-inflammatory cytokine released from leukocytes and nonimmune cells, such as epithelial cells, and resolves inflammation and tissue injury, with monocytes and macrophages being the primary target.[52] Liraglutide-treated but not perindopril-treated Ins2^{Akita} mice displayed enhanced interleukin-10 protein expression in the kidney cortex (Figure 4c). The differentiation and polarization of macrophages into proinflammatory "M1" and anti-inflammatory "M2" states denote the 2 extreme maturation programs of macrophages during tissue injury.[53,54] Our data indicate that signaling through the GLP-1 pathway promotes an M2-like macrophage phenotype, suggestive of resolving inflammation.

Because of potential effects of liraglutide in resolving inflammation, we next investigated the possibility that this may be associated with effects on progenitor cells of the monocyte/macrophage lineage within the bone marrow. Flow cytometric analysis of bone marrow showed a diabetes-induced expansion of bone marrow–derived hematopoietic stem and multipotent progenitor cells (Figure 4d), granulocyte macrophage progenitor cells (Figure 4e), and common myeloid progenitor cells (Figure 4f), all of which were attenuated with administration of liraglutide, but not with perindopril. Together, these data demonstrate the anti-inflammatory nature of liraglutide, which extends to a reduction in the extent of enhanced myelopoiesis in the bone marrow and an inflammation-resolving macrophage phenotype in the local renal microenvironment.

We next examined the consequences of loss of GLP-1R signaling on these parameters. Kidney cortical nuclear factor κB (p65) DNA-binding activity and kidney cortical MCP-1 protein expression were increased *Glp1r*$^{-/-}$ mice compared with their WT counterparts (Supplementary Figure S5A and B). Flow cytometric analysis of bone marrow showed an expansion of bone marrow–derived hematopoietic stem and multipotent progenitor cells (Supplementary Figure S5C), granulocyte macrophage progenitor cells (Supplementary Figure S5D), and a trend toward an increase in common myeloid progenitor cells (Supplementary Figure S5E, $P = 0.08$) in the *Glp1r*$^{-/-}$ versus WT mice revealing a proinflammatory renal phenotype and dysregulated hematopoiesis in mice with loss of GLP-1R signaling.

Transcriptional profiling at the single-cell level reveals a unique expression network in the kidney in response to pharmacologic activation of GLP-1R signaling

Given the cellular heterogeneity of the kidney, single-cell sequencing was used to map the cell-specific transcriptional response to liraglutide administration in mice with DKD. We conducted an unbiased genome-wide expression profiling of individual cells freshly dissociated from the kidney of Ins2^{Akita} mice with and without 20 weeks of liraglutide therapy (Figure 5a). After initial quality filtering of demultiplexed counts, a combined 16,015 single-cell profiles across samples remained for further integration and clustering using the R package Seurat. Specific gene marker expression was examined to assign identity to clustered cell profiles, as shown in Figure 5b, including proximal tubule: (*Slc27a2*); endothelial: (*Emcn*); distal tubule: (*Slc12a3*); podocyte: (*Nphs1*); loop Henle: (*Slc12a1*); macrophage: (*Cd68*); collecting duct (intercalated): (*Atp6v0d2*); collecting duct (principal): (*Hsd11b2*); B-lymphocytes: (*Cd79a*); T-lymphocyte/N-killer: (*Cd3g*), Gzma; mesangial: (*Myl9*); neutrophil: (*S100a8*); juxtaglomerular/granular: (*Ren1*). Fifteen distinct clusters were identified and mapped according to gene expression representing the major cell types found in the kidney,[55,56] including several immune cell types (Figure 5c). Cluster distribution by the experimental group (Figure 5d) showed that each group contributed cells to every cluster, indicating the absence of dissociation bias. There was no change in the cell number in mice with diabetes after treatment with liraglutide compared with diabetic mice (Figure 5e). Overall, the heat map illustrates that liraglutide rescued gene expression changes induced by DKD across all major renal cell types (Figure 5f).

Distinct cell types responded differently to liraglutide (Figure 6a). For example, fatty acid–binding protein-4 (*Fabp4*) was upregulated in endothelial cells in DKD and downregulated by liraglutide (Figure 6a), but this change was not identified in other cell types. The top differentially expressed gene (DEG) in proximal tubular cells in DKD was DEPP1 autophagy regulator (8430408G22Rik), and this was reduced in mice treated with liraglutide (Figure 6a). In podocytes, *Ndufs5*, a subunit of mitochondrial complex I of the

Figure 3 | (continued) measured by the ELISA. (**d**) Glomerular sclerotic index (GSI) histology score. GSI was quantitated using periodic acid–Schiff (PAS) staining and light microscopy under original magnification of ×400. (**e**) Representative PAS-stained kidney sections. Original magnification ×400 and Bar = 25 μm. (**f**) Representative transmission electron micrographs (viewed at original magnification ×3000) of glomerular podocytes demonstrating thickening of the glomerular basement membrane (GBM, orange arrows) in Ins2^{Akita} mice compared with the wild-type (WT) control and prevention by liraglutide. Images also show change in podocyte foot processes (Bar = 2 μm). (**g**) GBM thickness. (**h**) Podocyte foot processes per 100 μm GBM. (**i**) Urinary kidney injury molecule (KIM)-1 as determined by the ELISA in 24-hour urine collections. (**j**) Activated transforming growth factor-β1 (TGF-β1) protein in the kidney cortex. (**k**) Fibronectin in glomeruli by immunohistochemistry. (**l**) Representative images (Bar = 25 μm). Data are presented as mean ± SD (n = 3–12 per group). Dots represent individual mice. *P* values were determined by 1-way analysis of variance with the Tukey multiple comparison test. *$P < 0.05$, **$P < 0.01$, ***$P < 0.001$, ****$P < 0.0001$. ACEi, Ins2^{Akita} perindopril; Con, WT; Lira, Ins2^{Akita} liraglutide; L + A, Ins2^{Akita} liraglutide + perindopril; Veh, Ins2^{Akita} vehicle; WOA, week of age. To optimize viewing of this image, please see the online version of this article at www.kidney-international.org.

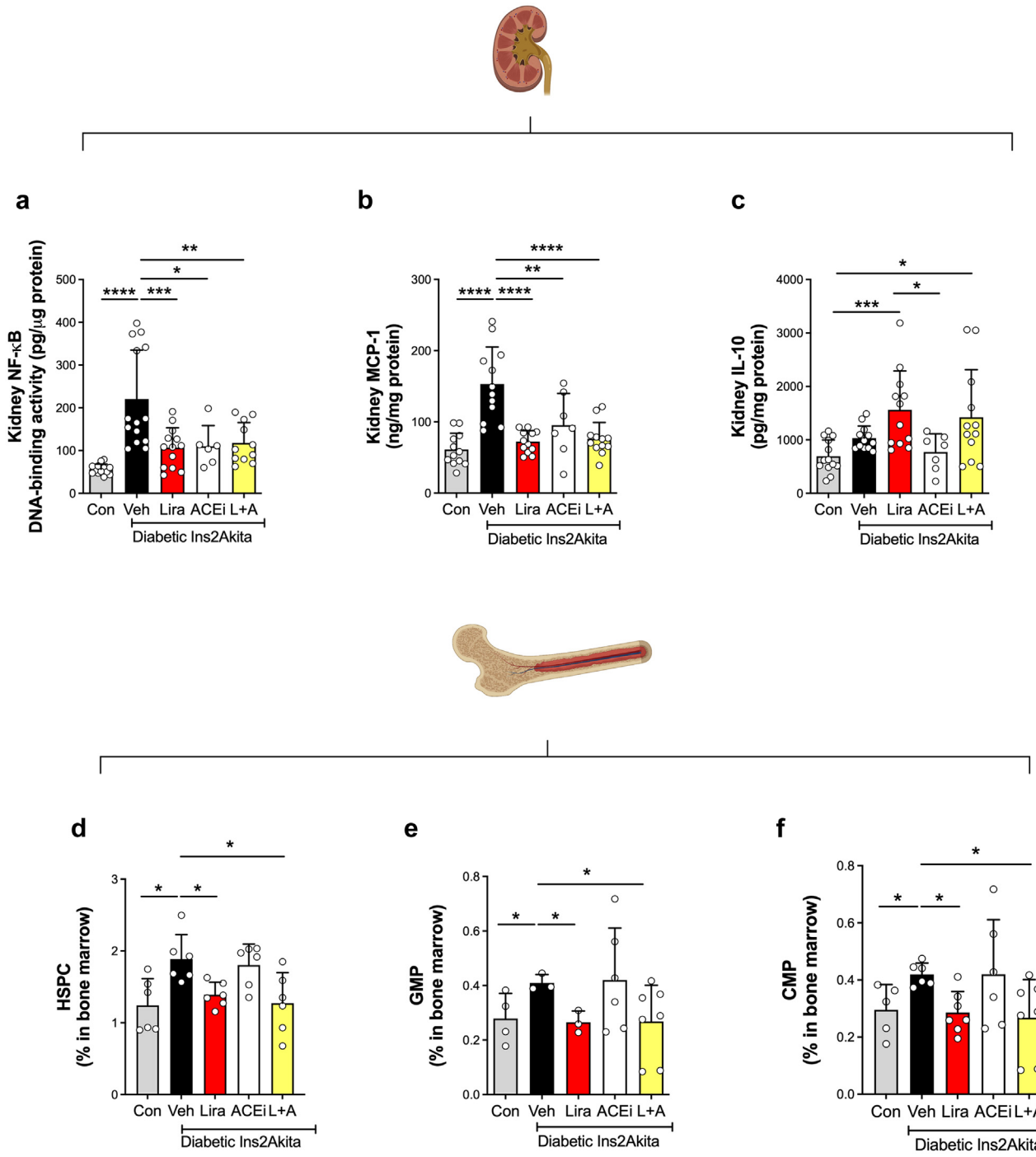

Figure 4 | Liraglutide attenuates receptor for advanced glycation end product (RAGE)-mediated myelopoiesis and influences macrophage polarization, dampening kidney inflammation. Ins2^{Akita} mice were treated with liraglutide, the angiotensin-converting enzyme inhibitor (ACEi) perindopril, or a combination of liraglutide and perindopril for 20 weeks. (**a**) Nuclear factor κB (NF-κB) DNA-binding activity in the kidney cortex. (**b**) Kidney monocyte chemoattractant protein (MCP)-1 protein. (**c**) Kidney interleukin (IL)-10 protein. Bone marrow–derived progenitor cells were measured by flow cytometry: (**d**) hematopoietic stem and multipotent progenitor cells (HSPC), (**e**) granulocyte macrophage progenitor cells (GMP), and (**f**) common myeloid progenitor cells (CMP). Data are presented as mean ± SD (n = 4–12 per group). Dots represent individual mice. *P* values were determined by 1-way analysis of variance with the Tukey multiple comparison test. $^{*}P < 0.05$, $^{**}P < 0.01$, $^{***}P < 0.001$, $^{****}P < 0.0001$. ACEi, Ins2^{Akita} perindopril; Con, WT; Lira, Ins2^{Akita} liraglutide; L + A, Ins2^{Akita} liraglutide + perindopril; Veh, Ins2^{Akita} vehicle.

respiratory chain, was downregulated in DKD and restored with liraglutide (Figure 6a). To gain biological insight into the gene expression data, gene set enrichment analysis was performed. This revealed that liraglutide therapy induced changes in genes participating in a number of inflammatory, metabolic, and redox sensing pathways, which were altered

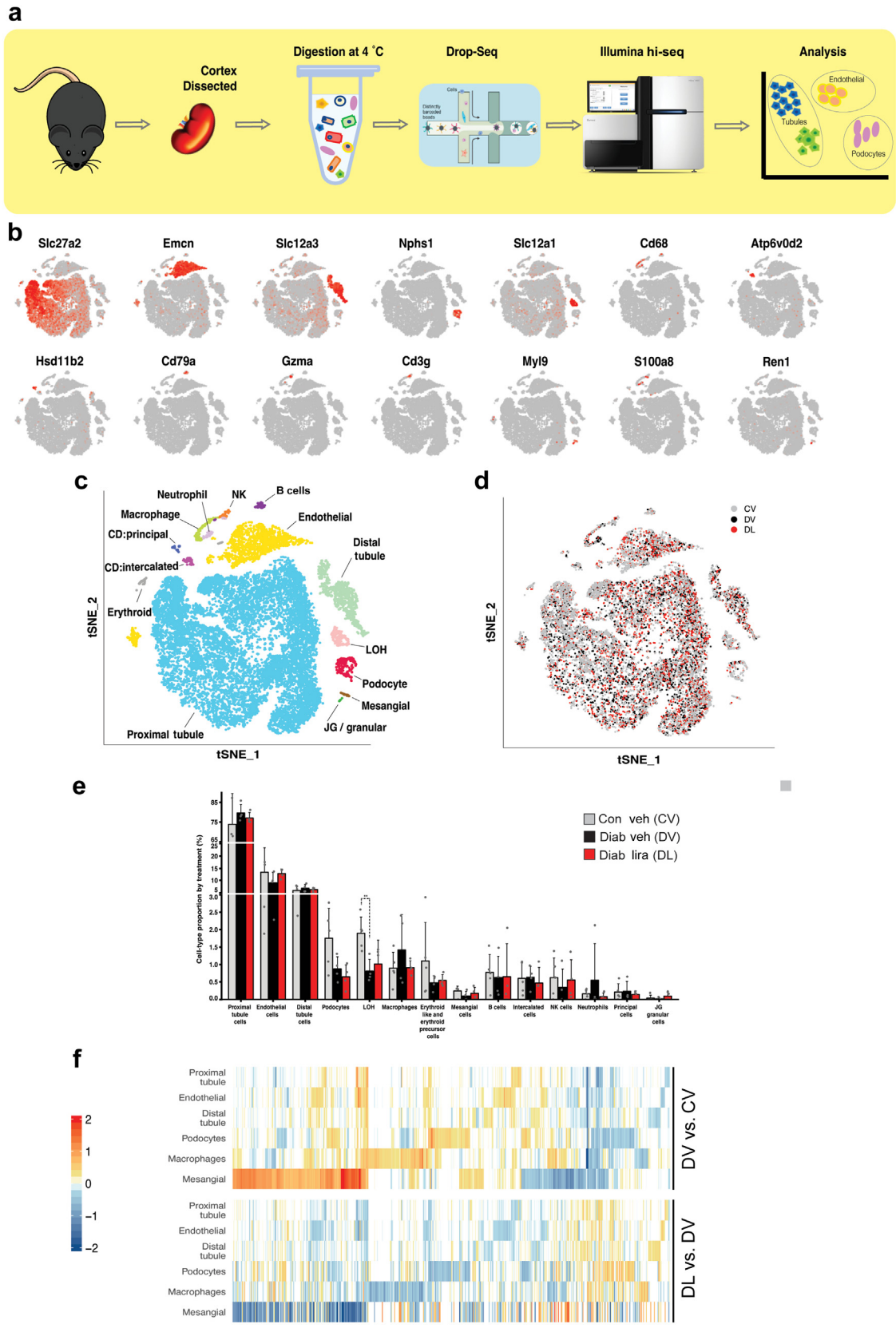

Figure 5 | Liraglutide remodels the kidney transcriptional network in diabetes. Single-cell RNA sequencing was performed to distinguish kidney cell populations in $Ins2^{Akita}$ mice treated with Lira. Cells were captured and visualized by t-distributed stochastic neighbor embedding (tSNE). (**a**) Workflow of renal single-cell RNA sequencing data creation. (**b**) Cluster identities verified by the expression of specific marker genes including proximal tubule: *Slc27a2*, endothelial: Emcn, distal tubule: Slc12a3, podocyte: Nphs1, loop of Henle (LOH): Slc12a1, (continued)

with diabetes (Figure 6b). Pathways induced by diabetes and suppressed by liraglutide included, among others, heat-shock protein signaling, mitochondrial metabolic pathways consisting of pyruvate metabolism and citric acid cycle, mitochondrial fatty acid β-oxidation, respiratory electron transport, and complex I biogenesis (Figure 6b). This mitochondrial signature was dominant in endothelial cells and proximal tubular cells. In addition, FOXO-mediated gene transcription and the solute-carrier gene superfamily pathways were dampened by liraglutide. Inflammasome pathways were also modulated by liraglutide therapy, with *Il1b* in natural killer cells decreasing, and distinct to macrophages, liraglutide rescued the diabetes-induced CLEC7A/inflammasome and NLRP3-inflammasome pathways (Figure 6b). The podocyte also displayed an inflammatory signature that was partly remodeled with liraglutide (Supplementary Figure S6). Supplementary Figure S7 shows the top 200 differentially expressed genes in the podocyte in response to liraglutide. Next, we wanted to see which cell types expressed *Ager* and *Glp1r*. *Ager* was detected in the $Ins2^{Akita}$ mouse kidney in endothelial cells, proximal tubular cells, distal tubular cells, and most predominantly, the podocytes (Supplementary Figure S8), with increased expression compared with control. Liraglutide treatment downregulated *Ager* in all of these cell types except endothelial cells. Interestingly, liraglutide led to an upregulation of *Ager* in B cells (Supplementary Figure S8). *Glpr1r* was below the limit of detection in our single-cell sequencing analysis.

We next explored some of the over-represented pathways highlighted by gene set enrichment analysis, which were downregulated in diabetes and restored in diabetic mice treated with liraglutide (Figure 6b). Gene networks relating to the resolution of inflammation predominated, including pathways such as interleukin-15 signaling and the heat shock protein 90 chaperone cycle for steroid hormone receptors, with *Hsp90ab1* expression restored by liraglutide, and ATF6 (activating transcription factor 6 alpha) activates chaperone genes, prolactin receptor signaling, activation of BAD and translocation to mitochondria, Tie2 signaling, vascular endothelial growth factor receptor-2–mediated vascular permeability, and binding and uptake of ligands by scavenger receptors (Figure 6b).

A spreadsheet summarizing the DEGs across experimental groups by cell cluster can be found in Supplementary Data File 2. Of particular interest was the identification of the following 3 genes: *Slc6a19*, *Txnip*, and *Slc11a1* (Figure 6c). The *Slc6a19* transcript level was increased in diabetes and decreased after liraglutide treatment (Figure 6c). *Slc11a1* was upregulated uniquely in the macrophage cell population in diabetes and was decreased with liraglutide treatment (Figure 6c). *Txnip* was a key signaling node reflected across proximal tubule cells, podocytes, macrophages, and endothelial cells in the $Ins2^{Akita}$ mouse and was downregulated by liraglutide (Figure 6c). This expression pattern was verified in the kidney cortex using targeted quantitative polymerase chain reaction (Figure 6d). Consistent with redox regulation, *Depp/Depp1/c10orf10* was induced in diabetes and reduced with liraglutide treatment in several cell clusters, notably proximal tubule cells (Supplementary Figure S9).

Liraglutide provides kidney protection and dampens RAGE activation in a nondiabetic rodent model of chronic kidney disease

We next aimed to corroborate these findings in a nondiabetic model of kidney injury, the subtotal nephrectomized (SNx) rat. Eight-week-old Fisher rats underwent Sham or 5/6 nephrectomy and were treated for 7 weeks after surgery with liraglutide 0.2 mg/kg twice daily subcutaneously,[42] or phosphate-buffered saline vehicle (n = 6–12 per group) (Figure 7a). A small difference in body weight was observed in the Sham + Lira, SNx, and SNx + Lira group relative to the Sham group (Figure 7b). There was no change in glucose control as evidenced by glycated hemoglobin, thus indicating that any benefits to the kidney seen in this model were independent of changes in glycemia (Figure 7c). Left kidney weight to body weight ratio was elevated in both the SNx and SNx + Lira groups relative to the Sham groups (Figure 7d). Systolic blood pressure was elevated in the nephrectomized rats and not altered with liraglutide therapy (Figure 7e). Albuminuria (Figure 7f) and urinary albumin-creatinine ratio (Figure 7g) were increased in nephrectomized rats, and urine albumin-creatinine ratio was reduced by liraglutide. Likewise, plasma creatinine was increased in the SNx model; however, there was no change with liraglutide (Figure 7h). An increase in urinary KIM-1 was evident in nephrectomized rats, and this was decreased with liraglutide therapy (Figure 7i). Glomerulosclerosis was increased in the SNx group and improved with liraglutide (Figure 7j). We next assessed whether the renal structural and functional changes seen in the SNx groups were associated with changes in local RAGE expression in the kidney. The SNx group exhibited increased kidney RAGE protein expression relative to Sham, and this was prevented by liraglutide therapy (Figure 7k and l), demonstrating RAGE suppression by liraglutide in the absence of diabetes.

Figure 5 | (continued) macrophage: *Cd68*, collecting duct (CD) (intercalated): *Atp6v0d2*, collecting duct (principal): *Hsd11b2*, B-lymphocytes: *Cd79a*, T-lymphocyte/N-killer: *Cd3g*, Gzma, mesangial: *Myl9*, neutrophil: *S100a8*, and juxtaglomerular (JG)/granular: *Ren1*. Red indicates the detection of gene expression, and gray indicates no expression/below the limit of detection. (**c**) Cluster identity mapping according to the expression of marker genes. (**d**) Cluster distribution by the experimental group (Control + Vehicle [CV], Diabetic + Vehicle [DV], and Diabetic + liraglutide [DL]). (**e**) Cell counts (percentages) in renal cell populations from single-cell transcriptomic analysis in WT and $Ins2^{Akita}$ mice with and without liraglutide treatment. Data are displayed as mean ± SD (n = 4 mice/group). *$P < 0.05$. (**f**) Heat map of gene expression changes in proximal tubule cells, endothelial cells, distal tubule cells, podocytes, macrophages, and mesangial cells in vehicle-treated mice (top) versus liraglutide-treated mice (bottom). *P* values were determined by 1-way analysis of variance with the Tukey multiple comparison test. *$P <$ 0.05. CV, WT control vehicle; DL, $Ins2^{Akita}$ liraglutide; DV, $Ins2^{Akita}$ vehicle; NK, natural killer; WT, wild type.

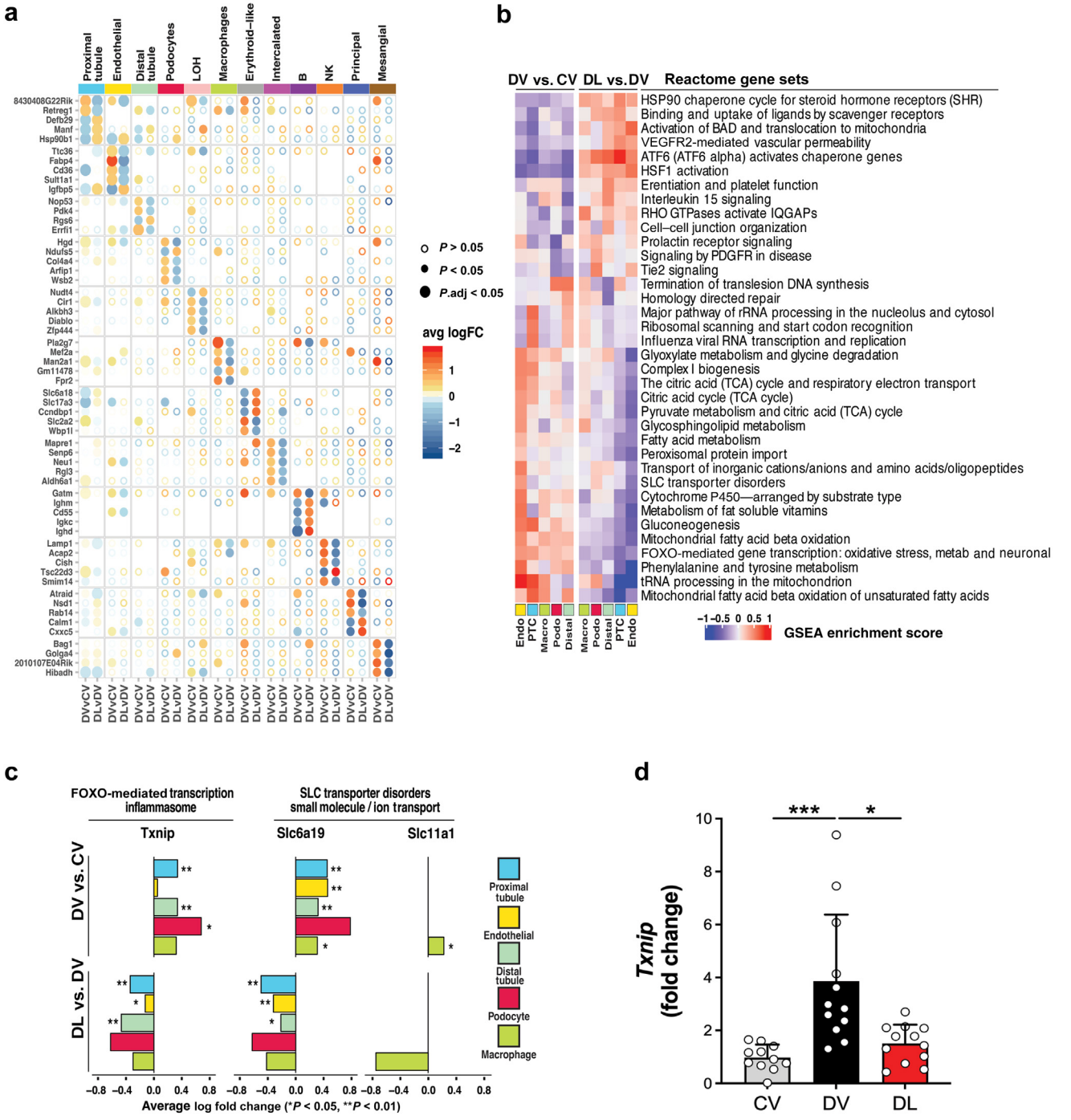

Figure 6 | Gene set enrichment analysis (GSEA) reveals novel pathways influenced by liraglutide in diabetic kidney disease (DKD). (**a**) Dot plot depicting top 5 cell-specific, upregulated, and downregulated genes during DKD ($Ins2^{Akita}$ vehicle, DV vs. control vehicle, CV) and in response to liraglutide in diabetes ($Ins2^{Akita}$ liraglutide, DL vs. DV). Color gradient indicates DEG enrichment score whereby red = higher expression and blue = lower expression of set genes. (**b**) Reactome GSEA of differential expression for the effect of diabetes "DV versus CV" and the effect of liraglutide in diabetes "DL versus DV" for clusters including proximal tubule, distal tubule, endothelial, podocyte, and macrophage. Color gradient indicates GSEA enrichment score, whereby red = higher expression and blue = lower expression of set genes. (**c**) Bar plots showing differential expression of specific genes including *Txnip*, *Slc6a19*, and *Slc11a1*. Bars indicate average log fold change (logFC) for contrasts of diabetes "DV versus CV" and the effect of liraglutide in diabetes "DL versus DV" across 5 cell types. (**d**) *Txnip* by quantitative polymerase chain reaction in the total kidney cortex. Data are presented as mean ± SD (n = 11–12 per group). Dots represent individual mice. *P* values were determined by 1-way analysis of variance with the Tukey multiple comparison test. $^{*}P < 0.05$, $^{***}P < 0.001$. ATF6, activating transcription factor 6; DEG, differentially expressed gene; GTPases, guanosine triphosphatases; HSF1, heat shock factor 1; HSP90, heat shock protein 90; LOH, loop of Henle; NK, natural killer; PDGFR, platelet-derived growth factor receptor; PTC, proximal tubular cell; SLC, solute carrier; VEGFR2, vascular endothelial growth factor receptor-2.

DISCUSSION

This study has demonstrated that GLP-1R signaling is an important pathway for controlling nonresolving inflammation in the kidney during diabetes and that loss of the GLP-1R leads to RAGE activation, inflammation, and kidney disease. Ablation of the GLP-1R caused progressive chronic kidney disease, which was accompanied by marked kidney RAGE upregulation and enhanced susceptibility to DKD. Kidney injury in *Glp1r*$^{-/-}$ mice could be rescued by RAGE deletion. GLP-1R agonism with liraglutide suppressed kidney RAGE expression and improved kidney injury in 2 distinct models of progressive chronic kidney disease, independent of glucose lowering. In mice with experimental diabetes, GLP-1R agonism reduced the expansion of bone marrow myeloid progenitor cells, promoted M2-like macrophage polarization, and suppressed inflammasome activation. GLP-1R agonism also led to signals of metabolic adaptation and tissue repair across key kidney cell populations. Collectively, these results identify novel pathways of kidney repair for GLP-1R agonism.

GLP-1RA are effective blood glucose–lowering therapies that are transforming the management of type 2 diabetes with an associated reduction in DKD and cardiovascular disease risk;[57,58] however, their mechanisms of action in reducing end-organ injury are incompletely understood. Given the impressive clinical responses to GLP-1RA therapy, understanding the central mechanisms by which incretins alter metabolism, including within the kidney, is of critical importance. The current study aimed to characterize the role of GLP-1 in kidney function, and indeed GLP-1 was found to be crucial for kidney homeostasis. We showed that mice with genetic disruption of *Glp1r* spontaneously develop renal injury exhibited by albuminuria, glomerular hyperfiltration, and fibrosis. When diabetes was chemically induced in *Glpr1r*-deficient mice, kidney injury was accelerated, beyond that observed in diabetic WT mice, as reflected by albuminuria and worsening DKD. Taken together, these findings confirm a role for the endogenous GLP-1R in conferring susceptibility to kidney injury.

We then showed that the development of STZ diabetes was associated with an increase in kidney RAGE expression and a decrease in GLP-1R expression. The deletion of RAGE (RAGE KO mice) prevented the decrease in GLP-1R, whereas *Glp1r*$^{-/-}$ mice showed RAGE upregulation, demonstrating cross-talk between these 2 pathways. To further explore regulation of these pathways *in vivo*, we generated a dKO mouse model where both RAGE and GLP-1R were deleted. The dKO mice exhibited a similar renoprotective phenotype to that of the RAGE KO mouse alone. This suggests that preventing RAGE signaling in the absence of GLP-1 is protective, emphasizing a dominant role for RAGE in DKD progression. Indeed, there is a large body of clinical and experimental evidence that the AGE-RAGE axis contributes to the onset and progression of DKD. We confirmed that genetic deletion of RAGE affords renoprotection, leading to reduced inflammation and fibrosis, as previously shown by our group and others.[23–25,59]

We next characterized changes in the kidney in response to therapy with a GLP-1RA used at a dose that did not reduce blood glucose. We identified that GLP-1R agonism with liraglutide confers renoprotection in an experimental model of insulin-deficient diabetes (Ins2^{Akita}) as well as in a nondiabetic model of renal fibrosis (SNx). This renoprotection was independent of blood glucose control and was as good as conventional treatments such as ACE inhibition, as achieved by perindopril. Our experimental findings are in agreement with the LEADER study, where liraglutide reduced the development and progression of DKD in patients with type 2 diabetes.[60] Similar findings with respect to renoprotection have been reported with other GLP-1RA, such as in the REWIND study with dulaglutide,[61] in the SUSTAIN program with semaglutide[62] and more recently the AMPLITUDE-O trial that used efpeglenatide.[57,63] With positive renal findings with GLP-1RA in numerous clinical trials albeit not performed primarily for renal endpoints, this has led to the commencement of dedicated trials enrolling people at risk for DKD such as the FLOW study (NCT03819153) to further define the role of these drugs as renoprotective therapies.

In the Ins2^{Akita} mouse model, liraglutide led to an increase in GLP-1R protein in the kidney, PKA activation, and suppressed RAGE expression. Liraglutide was efficacious against diabetes-associated albuminuria, glomerulosclerosis, renal fibrosis, and podocyte injury, including ultrastructural changes, exhibited by reducing GBM thickening. These data are consistent with previous studies by Kodera *et al.*,[10] who demonstrated renoprotective actions of the GLP-1 agonist, exendin-4, in a rat model of insulin-deficient diabetes in the absence of glucose lowering. Similarly, Fujita *et al.*[11] have shown that a 4-week treatment of liraglutide in young KK/Ta-Akita mice led to a reduction in the urinary albumin-to-creatinine ratio, although these previous experimental studies failed to elucidate an underlying mechanism at either a molecular or cellular level.

The effects of liraglutide on DKD in the Ins2^{Akita} mouse extended to a reduction in inflammation within the kidney, with suppression of nuclear factor κB DNA-binding activity and MCP-1 protein expression, whereas interleukin-10 protein was increased, indicating that signaling through the GLP-1 pathway promotes an M2-like macrophage phenotype in the kidney, suggestive of resolving inflammation. These results are supported by data from single-cell sequencing that revealed that liraglutide treatment in diabetic mice led to a dampening of inflammatory signals in macrophages. This resolving inflammation was accompanied by a reduction in myelopoiesis in the bone marrow. Together, these data confirm the anti-inflammatory nature of liraglutide systemically via direct effects on myelopoiesis and on M2-like macrophage polarization in the local renal microenvironment.

Because the kidney houses diverse cell populations,[64] we used unbiased single-cell RNA sequencing to explore the cellular landscape in response to a long-term GLP-1-incretin stimulus. Our data complement a recent and elegant study mapping the early single-cell transcriptomic response of mouse DKD to the other key therapies of DKD, including sodium-glucose

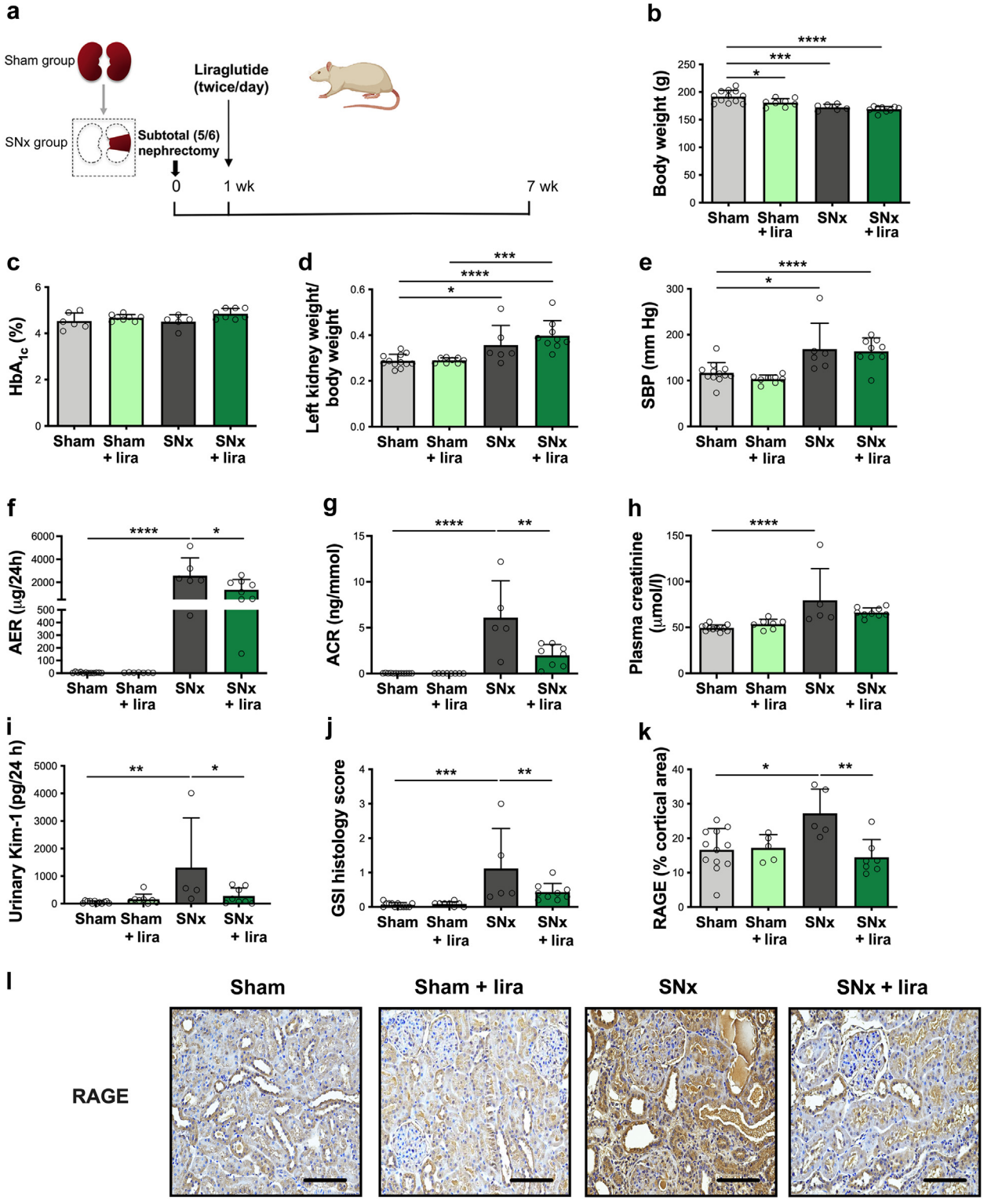

Figure 7 | The effects of liraglutide on receptor for advanced glycation end products (RAGE) and microvascular injury were corroborated in the subtotal nephrectomized (SNx) rat model. (**a**) Fisher rats were subjected to subtotal (5/6) nephrectomy and followed for 7 weeks with or without liraglutide (0.2 mg/kg twice daily subcutaneously), (**b**) body weight, (**c**) glycated hemoglobin (HbA_{1c}), (**d**) left kidney weight to body weight ratio, (**e**) systolic blood pressure (SBP), (**f**) albumin excretion rate (AER), (**g**) albumin-to-creatinine ratio (ACR), (**h**) plasma creatinine, (**i**) urinary kidney injury molecule (KIM)-1 measured, (**j**) glomerular sclerotic index (GSI) histology score, (**k**) RAGE protein in the kidney cortex by immunohistochemistry, and (**l**) representative images of RAGE staining within the kidney cortex. Original magnification ×400 and Bar = 25 µm. Data are presented as mean ± SD (n = 6–12 per group). Dots represent individual mice. *P* values were determined by 1-way analysis of variance with the Tukey multiple comparison test. *$P < 0.05$, **$P < 0.01$, ***$P < 0.001$, ****$P < 0.0001$. To optimize viewing of this image, please see the online version of this article at www.kidney-international.org.

cotransporter-2 inhibitors, rosiglitazone, and ACE inhibition.[65] In the current study, single-cell RNA sequencing identified clusters comprising endothelial, proximal tubule, podocyte, and macrophage cells influenced by pharmacologic GLP-1 signaling, associated with pathways involved in nutrient utilization, redox sensing, and resolution of inflammation. Our studies show that, independent of whole-body metabolism, GLP-1RA have effects on kidney nutrient utilization, inducing a shift toward kidney fatty acid metabolism that was particularly apparent in endothelial cells and proximal tubular cells. This was supported by a signal of increased mitochondrial complex I biogenesis and apparent flux through the mitochondrial respiratory chain in these cells, signals that were largely absent in podocytes. Fatty acids are the preferred energy source for kidney tubules, which are then metabolized by fatty acid oxidation and oxidative phosphorylation. Disturbances in kidney fatty acid metabolism have been observed in DKD.[66–68] In diabetes, the inability to make appropriate metabolic adaptations in the diabetic milieu leads to dysfunctional mitochondria and impaired renal energy generation. In DKD, there is a shift from oxidative phosphorylation[69,70] to glycolysis[71] via the Crabtree[72] or the Warburg[69] effect. An upregulation in "mitochondrial pathways" observed in the gene set enrichment analysis in our study is likely to reflect a shift in metabolism in the kidney in diabetes. However, live respiration studies would be required to determine mitochondrial function to directly assess if such changes in renal metabolism occurred in response to GLP1R agonism. This upregulation in "mitochondrial pathways" is likely a compensatory response to the increased metabolic demands of diabetes. Liraglutide reversed this mitochondrial signature in proximal tubular cells and endothelial cells. This could infer metabolic reprogramming by liraglutide and is likely due to a shift from glucose oxidation to lipid fueling, in an attempt to establish normal kidney metabolism.

GLP-1R agonism in diabetes also remodeled a network of nutrient transporters including *Slc6a19*, which encodes the sodium-dependent neutral amino acid transporter. The sodium-dependent neutral amino acid transporter is primarily expressed in early proximal tubules (S1–S2) and reabsorbs neutral amino acids.[73,74] The *Slc6a19* transcript level was increased in diabetes across most key cell populations and decreased after liraglutide treatment. A recent study found that mice with a deletion in *Slc6a19* were protected against aristolochic acid–induced nephropathy.[75] Of note, there is current interest in considering the sodium-dependent neutral amino acid transporter as a therapeutic target in diabetes.[76]

Slc11a1 is a member of the solute carrier family 11 (proton-coupled divalent metal ion transporters) and encodes a multipass membrane protein known as natural resistance-associated macrophage-1.[77,78] Natural resistance-associated macrophage-1 functions as a divalent transition metal (iron and manganese) transporter. It regulates macrophage and neutrophil activity primarily in the setting of innate immunity.[79] *Slc11a1* was upregulated uniquely in the macrophage cell population in diabetes and was decreased with liraglutide treatment, pointing toward reshaping of macrophage metabolism. *Txnip* was a key signaling node reflected across proximal tubule cells, podocytes, macrophages, and endothelial cells in the $Ins2^{Akita}$ mouse and was significantly downregulated by liraglutide. We also demonstrated that liraglutide reduced *Txnip* in the renal cortex. These data show that TXNIP is a target of the GLP-1-incretin pathway. Consistent with redox regulation, *Depp/Depp1/c10orf10*, a key hypoxia-inducible gene and transcriptional target of FOXO3, was induced in diabetes and was reduced by liraglutide treatment, predominantly in proximal tubule cells. *Depp1* localizes to peroxisomes and mitochondria and impairs cellular reactive oxygen species detoxification,[80] and it is involved in the activation of FOXO3-dependent autophagy.[81] More recently, *Depp1* was found to regulate hepatic glucose and fat metabolism partly by fibroblast growth factor 21,[82] though to our knowledge, no prior data exist regarding its specific role in the kidney.

Although the current studies have focused on direct renal mechanisms, one cannot exclude that other pathways may also be involved, including effects on weight, lipids and fatty acid metabolism, renal metabolism, kidney perfusion, and hypoxia, as has been suggested.[83] In an inflammation-driven kidney murine model, liraglutide specifically regulated genes related to the renin-angiotensin-aldosterone system, sodium glucose transporters, vasoconstriction, proliferation, angiogenesis, fibrosis, and inflammation.[84] It should be noted that this study has several limitations including the reliance on whole-body KO animals precluding precise evaluation of kidney-specific versus systemic effects.

In conclusion, these studies identify a novel glucose-independent renoprotective action of GLP-1RA in DKD, which includes the suppression of nonresolving inflammation across key kidney cell populations. This work supports the impetus to not only consider GLP-1-based therapies in DKD but also as a novel approach in nondiabetic chronic kidney diseases. In addition, these data provide a valuable resource for exploring the cell-specific kidney transcriptional response to long-term GLP-1 analog administration in diabetes.

DISCLOSURE

MEC has received honoraria from companies making GLP-1 receptor agonists and DPP-4 inhibitors including Novo Nordisk. MTC has received consultancy fees from Visterra Inc. AA has received research support from Boehringer Ingelheim. He was a recipient of a Novo Nordisk Diabetes Innovation Award and has received consultancy fees and honoraria from Novo Nordisk. LBK, DBT, and AK are the employees of Novo Nordisk. CH is past Novo Nordisk employee. LBK and DBT hold minor employee-based Novo Nordisk shares. DJD has received consulting or lecture honoraria from Altimmune, Amgen, Boehringer Ingelheim, Eli Lilly, Kallyope, Merck, Novo Nordisk, and Pfizer Inc. and Mt. Sinai Hospital has received investigator-initiated grant support from Amgen, Novo Nordisk, and Pfizer Inc. for studies in the Drucker Lab. All the other authors declared no competing interests.

DATA STATEMENT

The single-cell RNA sequencing data supporting the findings of this study are openly available in the Gene Expression Omnibus under accession GSE220045.

ACKNOWLEDGMENTS

We thank Dr. Benjamin J. Lamont, Dr. Sih Min Tan, Dr. Gavin C. Higgins, Dr. Matthew Snelson, Dr. Runa Lindblom, Ms. Tuong-Vi Nguyen, Ms. Jenny Wang, Ms. Sarah Rosli, Mrs. Maryann Arnstein, and Dr. Anna Watson for their technical assistance and Dr. Henrik Sondergaard (Novo Nordisk) for his contribution to these studies. We would like to thank Emeritus Professor George Jerums (Austin Health and the University of Melbourne, Department of Medicine) for his input into these studies. We acknowledge the assistance of the Clive and Vera Ramaciotti Centre for Structural Cryo-Electron Microscopy, Monash University, Australia. This work was completed with support from the Diabetes Australia Research Program (Y12V-SOUK), Novo Nordisk (584803), and the Victorian Government's Operational Infrastructure Support Program. KCS has been supported by the Diabetes Australia Research Trust Viertel Postdoctoral Fellowship and a Diabetes Australia Research Program grant. MTC is the recipient of a Career Development Award from JDRF Australia, the recipient of the Australian Research Council Special Research Initiative in Type 1 Juvenile Diabetes. MEC and JMF are recipients of NHMRC Investigator Grants. AE-O is an NHMRC Senior Research Fellow (1154650). DJD is supported in part by a Banting and Best Diabetes Centre-Novo Nordisk Chair and a Sinai Health-Novo Nordisk Foundation fund in regulatory peptides and CIHR grant 154321. Figures were created with BioRender.com.

AUTHOR CONTRIBUTIONS

KCS, YD, MTC, and MEC contributed equally to this work and are guarantors of this work. KCS is listed as first author because she was responsible for project management, overseeing the completion of all the experiments, running the mouse studies, analyzing the data, and completing all manuscript revisions. MTC is listed as last author as she supervised the experiments, analyzed the data and co-wrote the manuscript. KCS, YD, PK, MTC, and MEC each contributed to the conception and design of the study. KCS and YD conducted the experiments and analyzed the data. SSM and AE-O conducted the single-cell transcriptomic experiments and analysis. AJM and AA-s assisted with the bone marrow flow cytometric analysis. JMF, GR, SC, KJ-D, PK, MKM, CJR, SAP, and BEH assisted with the animal studies and drafting of the manuscript. DJD assisted with the provision of animals to establish colonies to complete the *in vivo* arm of the work. AA designed and ran the rat subtotal nephrectomy study and provided samples for further analysis. LBK, AK, DBT, and CH were involved in the study design. All of the authors have approved the final version of the manuscript.

SUPPLEMENTARY MATERIAL

Supplementary File (Word)

Supplementary Methods.

Supplementary Figure S1. No effect of genetic deletion of *Ager*, *Glp1r*, or both *Ager* and *Glp1r in vivo* on physiological or metabolic features at study endpoint. Wild-type (WT), $ager^{-/-}$, $Glp1r^{-/-}$, and *ager-glp1r* double knockout (dKO) mice were rendered diabetic with streptozotocin (STZ) and followed for 24 weeks. (**A**) Body weight, (**B**) food intake during 24-hour metabolic caging, (**C**) blood glucose, (**D**) glycated hemoglobin (HbA_{1c}), (**E**) water intake during 24-hour metabolic caging, and (**F**) urine output during 24-hour metabolic caging. Data are displayed as mean ± SD (n = 5–10 mice/group). Dots represent individual mice. $^{*}P < 0.05$, $^{**}P < 0.01$, $^{***}P < 0.001$, $^{****}P < 0.0001$. *P* values determined by 2-way analysis of variance with the Tukey multiple comparison test.

Supplementary Figure S2. Markers of glucagon-like peptide-1 receptor (GLP-1R) activation and oxidative stress in $Ager^{-/-}$, $Glp1r^{-/-}$, or *Ager-Glp1r* double knockout (dKO) mice. Wild-type (WT), $Ager^{-/-}$, $Glp1r^{-/-}$, and *Ager-Glp1r* dKO mice were rendered diabetic with streptozotocin (STZ) and followed for 24 weeks. (**A**) Protein kinase A (PKA) was determined in the kidney cortex by the enzyme-linked immunosorbent assay (ELISA). (**B**) 8-Isoprostanes as determined by the ELISA in 24-hour urine collections. Data are displayed as mean ± SD (n = 5–10 mice/group). Dots represent individual mice. $^{*}P < 0.05$, $^{**}P < 0.01$, $^{****}P < 0.0001$. *P* values determined by 2-way analysis of variance with the Tukey multiple comparison test.

Supplementary Figure S3. No effect of pharmacologic treatment with liraglutide, perindopril, or combination therapy (liraglutide and perindopril) on physiological or metabolic features at the study endpoint in $Ins2^{Akita}$ mice. (**A**) Blood glucose (glucometer), (**B**) glycated hemoglobin (HbA_{1c}), (**C**) food intake during 24-hour metabolic caging, (**D**) water intake during 24-hour metabolic caging, (**E**) urine output during 24-hour metabolic caging, and (**F**) body weight. Data are displayed as mean ± SD (n = 12 mice/group). Dots represent individual mice. $^{*}P < 0.05$, $^{**}P < 0.01$, $^{***}P < 0.001$, $^{****}P < 0.0001$. *P* values determined by 2-way analysis of variance with the Tukey multiple comparison test.

Supplementary Figure S4. Markers of glucagon-like peptide-1 receptor (GLP-1R) activation and receptor for advanced glycation end products (RAGE) in the kidney cortex in liraglutide-treated $Ins2^{Akita}$ mice. (**A**) *Glp1r* mRNA expression in the kidney cortex. (**B**) Protein kinase A (PKA) in the kidney cortex. (**C**) *Ager* mRNA expression in the kidney cortex. (**D**) RAGE protein in the kidney cortex. Data are displayed as mean ± SD (n = 11–12 mice/group). Dots represent individual mice. $^{**}P < 0.01$, $^{***}P < 0.001$, $^{****}P < 0.0001$. *P* values determined by 1-way analysis of variance with the Tukey multiple comparison test.

Supplementary Figure S5. Markers of inflammation in $Glp1r^{-/-}$ mice. (**A**) Nuclear factor κB (NF-κB) DNA-binding activity in the kidney cortex by the enzyme-linked immunosorbent assay (ELISA). (**B**) Kidney MCP-1 protein by the ELISA. (**C–E**) Bone marrow–derived progenitor cells were measured by flow cytometry: (**C**) hematopoietic stem and multipotent progenitor cells (HSPC), (**D**) granulocyte macrophage progenitor cells (GMP), and (**E**) common myeloid progenitor cells (CMP). Data are displayed as mean ± SD (n = 4–7 per group). Dots represent individual mice. *P* values were determined by an unpaired 2-tailed *t* test. $^{*}P < 0.05$, $^{***}P < 0.001$.

Supplementary Figure S6. Podocyte inflammatory signature. Differential expression (average log fold change [logFC]) of detected inflammation set genes (Reactome) in podocytes from mice with diabetes versus control (Ins2-Akita DV vs. Control CV) and diabetes versus diabetes plus liraglutide treatment (Ins2-Akita + Lira DL vs. Ins2-Akita DV). n = 4 mice per group.

Supplementary Figure S7. Top 200 differentially expressed genes in the podocyte in response to liraglutide. Top 200 differentially expressed genes in the podocyte cell population from single-cell transcriptomic analysis in Ins2-Akita mice with or without liraglutide treatment. Right-hand column follows on from left. n = 4 mice per group. Differentially expressed genes between groups were determined using Seurat FindMarkers with Wilcoxon rank-sum testing. *P* value adjustment is based on the Bonferroni correction using all genes in the dataset. DL, diabetic liraglutide; DV, Ins2Akita vehicle.

Supplementary Figure S8. Dot plot of *Ager* gene expression in Control versus Ins2-Akita mice with and without liraglutide treatment. *Ager* expression in kidney cell populations from single-cell transcriptomic analysis in Control (CV), Ins2-Akita mice (DV), and Ins2-Akita mice treated with liraglutide (DL). Data are displayed as percentage cells expressing *Ager*. The average expression level is scaled, where 0 is not detected and 1 represents highest expression detected for *Ager*. n = 4 mice per group.

Supplementary Figure S9. Liraglutide reverses the *Depp1* gene signature in diabetes. *Depp1* expression in kidney cell populations

from single-cell transcriptomic analysis in $Ins2^{Akita}$ mice with (top) or without (bottom) liraglutide treatment. Data are displayed as log2 normalized expression per cell per group (n = 4 mice per group). Dots represent individual cells. Differentially expressed genes between groups were determined using Seurat FindMarkers with Wilcoxon rank-sum testing. *P* value adjustment is based on the Bonferroni correction using all genes in the dataset. DL, diabetic liraglutide; DV, $Ins2^{Akita}$ vehicle.

Supplementary Table S1. Primer and probe sequences for quantitative reverse transcription polymerase chain reaction**.**

Supplementary References.

Supplementary File (Excel)

Supplementary Data File S2.

REFERENCES

1. Cooper ME. Pathogenesis, prevention, and treatment of diabetic nephropathy. *Lancet*. 1998;352:213–219.
2. Shaw JE, Sicree RA, Zimmet PZ. Global estimates of the prevalence of diabetes for 2010 and 2030. *Diabetes Res Clin Pract*. 2010;87:4–14.
3. Parving HH, Lewis JB, Ravid M, et al. Prevalence and risk factors for microalbuminuria in a referred cohort of type II diabetic patients: a global perspective. *Kidney Int*. 2006;69:2057–2063.
4. Thomas MC, Cooper ME, Zimmet P. Changing epidemiology of type 2 diabetes mellitus and associated chronic kidney disease. *Nat Rev Nephrol*. 2016;12:73–81.
5. Effect of intensive blood-glucose control with metformin on complications in overweight patients with type 2 diabetes (UKPDS 34). UK Prospective Diabetes Study (UKPDS) Group. *Lancet*. 1998;352:854–865.
6. UK Prospective Diabetes Study Group. Tight blood pressure control and risk of macrovascular and microvascular complications in type 2 diabetes: UKPDS 38. *BMJ*. 1998;317:703–713.
7. Writing Team for the Diabetes Control and Complications Trial/Epidemiology of Diabetes Interventions and Complications Research Group. Effect of intensive therapy on the microvascular complications of type 1 diabetes mellitus. *JAMA*. 2002;287:2563–2569.
8. Baggio LL, Drucker DJ. Biology of incretins: GLP-1 and GIP. *Gastroenterology*. 2007;132:2131–2157.
9. Dungan K, Buse JB. Glucagon-like peptide 1-based therapies for type 2 diabetes: a focus on exenatide. *Clin Diab*. 2005;23:56–62.
10. Kodera R, Shikata K, Kataoka HU, et al. Glucagon-like peptide-1 receptor agonist ameliorates renal injury through its anti-inflammatory action without lowering blood glucose level in a rat model of type 1 diabetes. *Diabetologia*. 2011;54:965–978.
11. Fujita H, Morii T, Fujishima H, et al. The protective roles of GLP-1R signaling in diabetic nephropathy: possible mechanism and therapeutic potential. *Kidney Int*. 2014;85:579–589.
12. Marso SP, Daniels GH, Brown-Frandsen K, et al. Liraglutide and cardiovascular outcomes in type 2 diabetes. *N Engl J Med*. 2016;375:311–322.
13. Gerstein HC, Colhoun HM, Dagenais GR, et al. Dulaglutide and renal outcomes in type 2 diabetes: an exploratory analysis of the REWIND randomised, placebo-controlled trial. *Lancet*. 2019;394:131–138.
14. Bierhaus A, Schiekofer S, Schwaninger M, et al. Diabetes-associated sustained activation of the transcription factor nuclear factor-kappaB. *Diabetes*. 2001;50:2792–2808.
15. Hofmann MA, Drury S, Fu C, et al. RAGE mediates a novel proinflammatory axis: a central cell surface receptor for S100/calgranulin polypeptides. *Cell*. 1999;97:889–901.
16. Kim W, Hudson BI, Moser B, et al. Receptor for advanced glycation end products and its ligands: a journey from the complications of diabetes to its pathogenesis. *Ann N Y Acad Sci*. 2005;1043:553–561.
17. Manigrasso MB, Juranek J, Ramasamy R, Schmidt AM. Unlocking the biology of RAGE in diabetic microvascular complications. *Trends Endocrinol Metab*. 2014;25:15–22.
18. Morcos M, Sayed AA, Bierhaus A, et al. Activation of tubular epithelial cells in diabetic nephropathy. *Diabetes*. 2002;51:3532–3544.
19. Wendt T, Tanji N, Guo J, et al. Glucose, glycation, and RAGE: implications for amplification of cellular dysfunction in diabetic nephropathy. *J Am Soc Nephrol*. 2003;14:1383–1395.
20. Wautier JL, Guillausseau PJ. Advanced glycation end products, their receptors and diabetic angiopathy. *Diabetes Metab*. 2001;27:535–542.
21. Bierhaus A, Humpert PM, Morcos M, et al. Understanding RAGE, the receptor for advanced glycation end products. *J Mol Med (Berl)*. 2005;83:876–886.
22. Schmidt AM, Hasu M, Popov D, et al. Receptor for advanced glycation end products (AGEs) has a central role in vessel wall interactions and gene activation in response to circulating AGE proteins. *Proc Natl Acad Sci U S A*. 1994;91:8807–8811.
23. Coughlan MT, Thorburn DR, Penfold SA, et al. RAGE-induced cytosolic ROS promote mitochondrial superoxide generation in diabetes. *J Am Soc Nephrol*. 2009;20:742–752.
24. Sourris KC, Morley AL, Koitka A, et al. Receptor for AGEs (RAGE) blockade may exert its renoprotective effects in patients with diabetic nephropathy via induction of the angiotensin II type 2 (AT2) receptor. *Diabetologia*. 2010;53:2442–2451.
25. Tan AL, Sourris KC, Harcourt BE, et al. Disparate effects on renal and oxidative parameters following RAGE deletion, AGE accumulation inhibition, or dietary AGE control in experimental diabetic nephropathy. *Am J Physiol Renal Physiol*. 2010;298:F763–F770.
26. Wendt TM, Tanji N, Guo J, et al. RAGE drives the development of glomerulosclerosis and implicates podocyte activation in the pathogenesis of diabetic nephropathy. *Am J Pathol*. 2003;162:1123–1137.
27. Myint KM, Yamamoto Y, Doi T, et al. RAGE control of diabetic nephropathy in a mouse model: effects of RAGE gene disruption and administration of low-molecular weight heparin. *Diabetes*. 2006;55:2510–2522.
28. Yamamoto Y, Kato I, Doi T, et al. Development and prevention of advanced diabetic nephropathy in RAGE-overexpressing mice. *J Clin Invest*. 2001;108:261–268.
29. Ishibashi Y, Matsui T, Takeuchi M, Yamagishi S-I. Glucagon-like peptide-1 (GLP-1) inhibits advanced glycation end product (AGE)-induced up-regulation of VCAM-1 mRNA levels in endothelial cells by suppressing AGE receptor (RAGE) expression. *Biochem Biophys Res Commun*. 2010;391:1405–1408.
30. Ishibashi Y, Nishino Y, Matsui T, et al. Glucagon-like peptide-1 suppresses advanced glycation end product-induced monocyte chemoattractant protein-1 expression in mesangial cells by reducing advanced glycation end product receptor level. *Metabolism*. 2011;60:1271–1277.
31. Muskiet MHA, Tonneijck L, Smits MM, et al. GLP-1 and the kidney: from physiology to pharmacology and outcomes in diabetes. *Nat Rev Nephrol*. 2017;13:605–628.
32. Skov J. Effects of GLP-1 in the kidney. *Rev Endocr Metab Disord*. 2014;15:197–207.
33. Dunphy JL, Taylor RG, Fuller PJ. Tissue distribution of rat glucagon receptor and GLP-1 receptor gene expression. *Mol Cell Endocrinol*. 1998;141:179–186.
34. Korner M, Stockli M, Waser B, Reubi JC. GLP-1 receptor expression in human tumors and human normal tissues: potential for in vivo targeting. *J Nucl Med*. 2007;48:736–743.
35. Pyke C, Heller RS, Kirk RK, et al. GLP-1 receptor localization in monkey and human tissue: novel distribution revealed with extensively validated monoclonal antibody. *Endocrinology*. 2014;155:1280–1290.
36. Campos RV, Lee YC, Drucker DJ. Divergent tissue-specific and developmental expression of receptors for glucagon and glucagon-like peptide-1 in the mouse. *Endocrinology*. 1994;134:2156–2164.
37. Percie du Sert N, Hurst V, Ahluwalia A, et al. The ARRIVE guidelines 2.0: updated guidelines for reporting animal research. *PLoS Biol*. 2020;18:e3000410.
38. Bierhaus A, Haslbeck KM, Humpert PM, et al. Loss of pain perception in diabetes is dependent on a receptor of the immunoglobulin superfamily. *J Clin Invest*. 2004;114:1741–1751.
39. Constien R, Forde A, Liliensiek B, et al. Characterization of a novel EGFP reporter mouse to monitor Cre recombination as demonstrated by a Tie2 Cre mouse line. *Genesis*. 2001;30:36–44.
40. Scrocchi LA, Brown TJ, MaClusky N, et al. Glucose intolerance but normal satiety in mice with a null mutation in the glucagon-like peptide 1 receptor gene. *Nat Med*. 1996;2:1254–1258.
41. Chen LH, Stead B, Advani SL, et al. Hyperglycemia and renal mass ablation synergistically augment albuminuria in the diabetic subtotally nephrectomized rat: implications for modeling diabetic nephropathy. *Nephron Extra*. 2012;2:115–124.

42. Cummings BP, Stanhope KL, Graham JL, et al. Chronic administration of the glucagon-like peptide-1 analog, liraglutide, delays the onset of diabetes and lowers triglycerides in UCD-T2DM rats. *Diabetes*. 2010;59:2653–2661.
43. Han WK, Bailly V, Abichandani R, et al. Kidney injury molecule-1 (KIM-1): a novel biomarker for human renal proximal tubule injury. *Kidney Int*. 2002;62:237–244.
44. Drucker DJ, Philippe J, Mojsov S, et al. Glucagon-like peptide I stimulates insulin gene expression and increases cyclic AMP levels in a rat islet cell line. *Proc Natl Acad Sci U S A*. 1987;84:3434–3438.
45. Ron D. Proteotoxicity in the endoplasmic reticulum: lessons from the Akita diabetic mouse. *J Clin Invest*. 2002;109:443–445.
46. Chang JH, Gurley SB. Assessment of diabetic nephropathy in the Akita mouse. *Methods Mol Biol*. 2012;933:17–29.
47. Nagareddy PR, Murphy AJ, Stirzaker RA, et al. Hyperglycemia promotes myelopoiesis and impairs the resolution of atherosclerosis. *Cell Metab*. 2013;17:695–708.
48. Lee YS, Jun HS. Anti-inflammatory effects of GLP-1-based therapies beyond glucose control. *Mediators Inflamm*. 2016;2016:3094642.
49. Sourris KC, Yao H, Jerums G, et al. Can targeting the incretin pathway dampen RAGE-mediated events in diabetic nephropathy? *Curr Drug Targets*. 2016;17:1252–1264.
50. Chen T, Cao Q, Wang Y, Harris DCH. M2 macrophages in kidney disease: biology, therapies, and perspectives. *Kidney Int*. 2019;95:760–773.
51. Baggiolini M. Chemokines and leukocyte traffic. *Nature*. 1998;392:565–568.
52. Iyer SS, Cheng G. Role of interleukin 10 transcriptional regulation in inflammation and autoimmune disease. *Crit Rev Immunol*. 2012;32:23–63.
53. Murray PJ. Macrophage Polarization. *Annu Rev Physiol*. 2017;79:541–566.
54. Lee H, Fessler MB, Qu P, et al. Macrophage polarization in innate immune responses contributing to pathogenesis of chronic kidney disease. *BMC Nephrol*. 2020;21:270.
55. Wilson PC, Wu H, Kirita Y, et al. The single-cell transcriptomic landscape of early human diabetic nephropathy. *Proc Natl Acad Sci U S A*. 2019;116:19619–19625.
56. Park J, Shrestha R, Qiu C, et al. Single-cell transcriptomics of the mouse kidney reveals potential cellular targets of kidney disease. *Science*. 2018;360:758–763.
57. Tommerdahl KL, Kendrick J, Bjornstad P. The role of glucagon-like peptide 1 (GLP-1) receptor agonists in the prevention and treatment of diabetic kidney disease: insights from the AMPLITUDE-O trial. *Clin J Am Soc Nephrol*. 2022;17:905–907.
58. Palmer SC, Tendal B, Mustafa RA, et al. Sodium-glucose cotransporter protein-2 (SGLT-2) inhibitors and glucagon-like peptide-1 (GLP-1) receptor agonists for type 2 diabetes: systematic review and network meta-analysis of randomised controlled trials. *BMJ*. 2021;372:m4573.
59. Harcourt BE, Sourris KC, Coughlan MT, et al. Targeted reduction of advanced glycation improves renal function in obesity. *Kidney Int*. 2011;80:190–198.
60. Mann JFE, Orsted DD, Brown-Frandsen K, et al. Liraglutide and renal outcomes in type 2 diabetes. *N Engl J Med*. 2017;377:839–848.
61. Gerstein HC, Colhoun HM, Dagenais GR, et al. Dulaglutide and cardiovascular outcomes in type 2 diabetes (REWIND): a double-blind, randomised placebo-controlled trial. *Lancet*. 2019;394:121–130.
62. Mann JFE, Hansen T, Idorn T, et al. Effects of once-weekly subcutaneous semaglutide on kidney function and safety in patients with type 2 diabetes: a post-hoc analysis of the SUSTAIN 1-7 randomised controlled trials. *Lancet Diabetes Endocrinol*. 2020;8:880–893.
63. Gerstein HC, Sattar N, Rosenstock J, et al. Cardiovascular and renal outcomes with efpeglenatide in type 2 diabetes. *N Engl J Med*. 2021;385:896–907.
64. Balzer MS, Rohacs T, Susztak K. How many cell types are in the kidney and what do they do? *Annu Rev Physiol*. 2022;84:507–531.
65. Wu H, Villalobos RG, Yao X, et al. Mapping the single-cell transcriptomic response of murine diabetic kidney disease to therapies. *Cell Metab*. 2022;34:1064–1078.e6.
66. Ducasa GM, Mitrofanova A, Mallela SK, et al. ATP-binding cassette A1 deficiency causes cardiolipin-driven mitochondrial dysfunction in podocytes. *J Clin Invest*. 2019;129:3387–3400.
67. Stadler K, Goldberg IJ, Susztak K. The evolving understanding of the contribution of lipid metabolism to diabetic kidney disease. *Current Diabetes Reports*. 2015;15:40.
68. Weinberg JM. Lipotoxicity. *Kidney Int*. 2006;70:1560–1566.
69. Zhang G, Darshi M, Sharma K. The Warburg effect in diabetic kidney disease. *Semin Nephrol*. 2018;38:111–120.
70. Czajka A, Malik AN. Hyperglycemia induced damage to mitochondrial respiration in renal mesangial and tubular cells: implications for diabetic nephropathy. *Redox Biol*. 2016;10:100–107.
71. Lopes de Melo JM, Laursen JC, Søndergaard-Heinrich N, et al. Increased mitochondrial proton leak and glycolysis in peripheral blood mononuclear cells in type-1-diabetes. *Heliyon*. 2022;8:e12304.
72. Darshi M, Tumova J, Saliba A, et al. Crabtree effect in kidney proximal tubule cells via late-stage glycolytic intermediates. *iScience*. 2023;26:106462.
73. Broer A, Klingel K, Kowalczuk S, et al. Molecular cloning of mouse amino acid transport system B0, a neutral amino acid transporter related to Hartnup disorder. *J Biol Chem*. 2004;279:24467–24476.
74. Broer S. Amino acid transport across mammalian intestinal and renal epithelia. *Physiol Rev*. 2008;88:249–286.
75. Navarro-Garrido A, Kim YC, Oe Y, et al. Aristolochic acid-induced nephropathy is attenuated in mice lacking the neutral amino acid transporter B(0)AT1 (Slc6a19). *Am J Physiol Renal Physiol*. 2022;323:F455–F467.
76. Cheng Q, Shah N, Broer A, et al. Identification of novel inhibitors of the amino acid transporter B(0) AT1 (SLC6A19), a potential target to induce protein restriction and to treat type 2 diabetes. *Br J Pharmacol*. 2017;174:468–482.
77. Cellier M, Govoni G, Vidal S, et al. Human natural resistance-associated macrophage protein: cDNA cloning, chromosomal mapping, genomic organization, and tissue-specific expression. *J Exp Med*. 1994;180:1741–1752.
78. Kishi F. Isolation and characterization of human Nramp cDNA. *Biochem Biophys Res Commun*. 1994;204:1074–1080.
79. Cunrath O, Bumann D. Host resistance factor SLC11A1 restricts *Salmonella* growth through magnesium deprivation. *Science*. 2019;366:995–999.
80. Salcher S, Hagenbuchner J, Geiger K, et al. C10ORF10/DEPP, a transcriptional target of FOXO3, regulates ROS-sensitivity in human neuroblastoma. *Mol Cancer*. 2014;13:224.
81. Stepp MW, Folz RJ, Yu J, Zelko IN. The c10orf10 gene product is a new link between oxidative stress and autophagy. *Biochim Biophys Acta*. 2014;1843:1076–1088.
82. Li W, Ji M, Lin Y, et al. DEPP/DEPP1/C10ORF10 regulates hepatic glucose and fat metabolism partly via ROS-induced FGF21. *FASEB J*. 2018;32:5459–5469.
83. Thomas MC. The potential and pitfalls of GLP-1 receptor agonists for renal protection in type 2 diabetes. *Diabetes Metab*. 2017;43(suppl 1):2S20–2S27.
84. Ougaard ME, Sembach FE, Jensen HE, et al. Liraglutide improves the kidney function in a murine model of chronic kidney disease. *Nephron*. 2020;144:595–606.

SUPPLEMENTARY MATERIALS FOR

GLP-1 receptor signaling modifies the extent of diabetic kidney disease through dampening RAGE-induced inflammation

Karly C. Sourris[1,2•], Yi Ding[2,3•], Scott S. Maxwell[1], Annas Al-sharea[2], Phillip Kantharidis[1], Muthukumar Mohan[1], Carlos J Rosado[1], Sally A. Penfold[2], Claus Haase[3], Yangson Xu[2], Josephine M. Forbes[4], Simon Crawford[5], Georg Ramm[5], Brooke E. Harcourt[6], Karin Jandeleit-Dahm[1], Andrew Advani[7], Andrew J. Murphy[2], Daniel B. Timmermann[8], Anil Karihaloo[9], Lotte Bjerre Knudsen[8], Assam El-Osta[1], Daniel J. Drucker[10], Mark E. Cooper[1#], Melinda T. Coughlan[1,2#]

This PDF file includes:

Supplementary Methods

Figures S1 to S9

Table S1

Supplementary Methods

Study approval

The animal use and welfare adhered to the guidelines of the National Health and Medical Research Council of Australia following protocols reviewed and approved by the Alfred Medical Research and Education Precinct Animal Ethics Committee (E/1449/2014/B, E/1791/2018/B, E/1263/2012B) or the guidelines of the Canadian Council on Animal Care and were approved by St. Michael's Hospital Animal Care Committee (ACC253).

Animal studies

All colonies were established (backcrossed >10 generations) and maintained at the Alfred Medical Research and Education Precinct Animal Services, Melbourne, Australia, unless otherwise stated. All rodents were housed in a temperature-controlled environment, with a 12-h light/12-h dark cycle, and had access to rodent chow (Specialty Feeds, Perth, Western Australia, Australia) and water *ad libitum*. The sample size was determined based on the pre-specified primary endpoint of albuminuria from previous studies performed in our laboratory using diabetic mouse models, taking into account a predicted 10% early death rate of diabetic mice.

Generation of RAGE x GLP-1R double KO mice

Mice deficient in either *Glpr1*, *Ager* or deficient in both *Ager* and *Glpr1* (*Ager-Glp1r*$^{-/-}$ double knockout) were generated on a C57BL/6J background (wild-type) (WT; C57BL/6J). *Ager*$^{-/-}$ mice were kindly donated by Prof Angelika Bierhaus, University of Heidelberg, Germany.[S1, S2] *Glp1r*$^{-/-}$ mice were kindly donated by Prof Daniel Drucker, University of Toronto, Canada. [S3] To generate the double knockout mice, *Ager*$^{-/-}$ mice were crossed with *Glp1r*$^{-/-}$ knockout mice. The resulting *Ager-Glp1r*$^{+-/+-}$ heterozygous mice were crossed and, after four generations, the *Ager-Glp1r*$^{-/-}$ mouse was generated,

and a colony established from these founders. The colony was maintained as *Ager-Glp1r*$^{+/+}$ heterozygous in order to obtain WT littermates.

Induction of Streptozotocin-induced diabetes

Groups of six-week-old (n=10-12/group) male mice were randomised to receive intraperitoneal injections of vehicle (sodium citrate buffer, pH4.5) or streptozotocin (55 mg/kg/day, Sigma-Aldrich, St. Louis, MO) for 5 consecutive days as previously described.[S4] On the sixth day, blood glucose was tested by Glucometer using Accu-Chek® Advantage II test strips (Roche Diagnostics GmbH, Mannheim, Germany) and only mice with a blood glucose reading >15 mmol/L were included (> 90% mice injected) within the diabetic groups of the study. After 24 weeks, animals received an overdose of sodium pentobarbital (80 mg/kg i.p.), followed by exsanguination by cardiac puncture and the kidneys were rapidly dissected, weighed, and snap-frozen or placed in 10% neutral buffered formalin (v/v) for fixation before paraffin embedding.

Ins2Akita mice

Diabetic Ins2Akita mice (C57BL/6-*Ins2*^{Akita}/J) and their WT counterparts were purchased from the Jackson Laboratory (Strain #003548, Bar Harbor, ME, USA) and a colony established. Since the *Ins2*^{Akita} mutation is autosomal dominant, with homozygotes for the Ins2Akita allele exhibiting failure to thrive and early death, the heterozygote mice are suitable to study. At 6 weeks of age, male WT or heterozygous Ins2Akita mice were randomly assigned to receive either vehicle (PBS-Tween 80), or liraglutide (Lira, 50μg/kg) by daily subcutaneous injection for 20 weeks (n=12 mice per group). The dose of liraglutide was chosen based on pilot studies which aimed to identify the highest dose which did not significantly influence glycaemic control (50 μg/kg/day). In addition, a group of heterozygous Ins2Akita mice were randomised to receive the current standard of care for individuals with DKD, the ACE-inhibitor perindopril (ACEi, 2mg/kg) provided in the drinking water; and a further group of heterozygous Ins2Akita mice were administered a combination therapy consisting of liraglutide and

perindopril (L+A) for 20 weeks (n=12 mice per group). Blood glucose and body weight were recorded on a weekly basis as part of animal routine monitoring. After 20 weeks, animals received an overdose of sodium pentobarbital (80 mg/kg i.p.), followed by exsanguination by cardiac puncture and the kidneys were rapidly dissected, weighed and snap-frozen, or placed in 10% neutral buffered formalin (v/v) for fixation before paraffin embedding.

Rat Sub-total Nephrectomy model

Female Fischer 344 rats (Charles River, Montreal, Quebec, Canada) aged 8 weeks were randomized to undergo subtotal nephrectomy (SNx) or sham surgery, as previously described.[S5] Briefly, animals were anaesthetized with 2.5% isoflurane, the right kidney was removed via a subcapsular nephrectomy and infarction of approximately two thirds of the left kidney was achieved via selective ligation of two out of the three or four branches of the left renal artery. Sham surgery consisted of laparotomy and manipulation of both kidneys before wound closure. One week after surgery, rats were randomized to receive liraglutide (Novo Nordisk Canada Inc., Mississauga, Ontario, Canada) 0.2mg/kg twice daily s.c. [S6] or PBS (n=6-12/group) for 7 weeks. Urine albumin excretion was determined using AssayMax Rat Albumin ELISA kit (Assaypro, St. Charles, MO) after 24h metabolic caging. Systolic blood pressure was determined in conscious rats using an occlusive tail-cuff plethysmograph attached to a pneumatic pulse transducer (Powerlab, ADInstruments, Colorado Springs, CO), as previously described. [S7] Plasma creatinine was determined by autoanalyzer. Hemoglobin A1c (Glycated haemoglobin) was measured using A1cNow+ (Bayer, Sunnyvale, CA). At sacrifice rat kidney tissue was collected and immersion-fixed in 10% neutral buffered formalin before processing, embedding in paraffin and sectioning.

Measurement of mouse physiological and biochemical parameters

One week prior to study completion, mice were individually placed in metabolic cages (Tecniplast®, Lane Cove, NSW, Australia) for a period of 24 hours. A blood sample was collected, body weight,

food and water intake monitored and urine collected. Glycated hemoglobin (GHb) was determined using a Cobas Integra 400 Autoanalyzer (Roche Diagnostics Corporation, USA). Systolic blood pressure (mmHg) was measured using a computerised non-invasive tail-cuff method (AD Instruments, Powerlab, Chart version 5.2.2, Bella Vista NSW, Australia) as previously described. [S8, S9]

Measurement of mouse kidney function

Albumin excretion rate (AER) was measured in 24-hour urine collections by a Mouse Albumin ELISA Quantitation Set (Cat. No. E90-134, Bethyl Laboratories Inc, Montgomery, TX, USA) as per the manufacturer's instructions. Creatinine was measured using the Creatinine plus ver.2 (CREP2) on a Cobas Integra 400 plus (Roche Diagnostics). Urinary Kim-1 (Kidney injury molecule-1) was measured by ELISA (USCN, Wuhan, China). Plasma Cystatin C was quantified by ELISA (Biovendor, Brno, Czech Republic).

Renal histology

Kidney sections (3μm) were stained with periodic-acid Schiff (PAS) and picrosirius red. Twenty glomeruli in each kidney were graded in a blinded fashion in accordance with the severity of glomerular damage. The degree of sclerosis in each glomerulus was subjectively graded on a scale of 0-4 with grade 0 = normal; grade 1 = sclerotic area up to 25% (minimal); grade 2 = sclerotic area 25-50% (moderate); grade 3 = sclerotic area 50-70% (moderate to severe), and grade 4 = sclerotic area 75-100% (severe). The GSI was then calculated using the following formula: GSI = (1 × n1) + (2 × n2) + (3 × n3) + (4 × n4)/n0 + n1 + n2 + n3 + n4, where nx is the number of glomeruli in each grade of glomerulosclerosis.

Immunohistochemistry

Paraffin sections of mouse kidney (4μm) were immunostained for fibronectin (Rabbit anti-human fibronectin, Cat#A024502, DAKO Cytomation, Glostrup, Denmark). Briefly, endogenous peroxidases

were blocked with 3% hydrogen peroxide for 15min and incubated in 0.5% skim milk/TBS for 1 hour at room temperature. Fibronectin slides underwent citrate buffer heat antigen retrieval. Primary antibody was left on overnight at 4ºC. This was followed by incubation with biotinylated secondary antibody for 10min at room temperature. Sections were then incubated with Vectastain ABC reagent (Vector Laboratories, CA, USA). Peroxidase activity was identified by reaction with 3,3'-diaminobenzidine tetrahydrochloride (Sigma-Aldrich Pty. Ltd, NSW, Australia). Sections were counterstained with haematoxylin. All sections were examined under light microscopy (Olympus BX-50; Olympus Optical) and digitized with a high-resolution camera. All digital quantitation (Image-Pro Plus, v6.0) and assessments were performed in a blinded manner.

Electron microscopy

Kidney biospecimens were dissected into 1 – 1.5 mm^3 cubes and placed into primary fixative, consisting of 2.5% glutaraldehyde and 2% paraformaldehyde in 0.1M sodium cacodylate buffer, for 1 hour at room temperature, followed by overnight incubation at 4ºC. Secondary fixation was performed using 1% osmium tetroxide and 1.5% potassium ferricyanide in cacodylate buffer for 1 hour at room temperature. The tissues were dehydrated in ethanol. Dehydrated tissues were incubated in a mixture of Epon resin and propylene oxide. The tissues were then placed into Beem capsules in 100% resin and the resin polymerised for 48 hours in an oven at 60ºC. Resin embedded tissue was sectioned with a Diatome diamond knife using a Leica UCS ultramicrotome (Leica, Port Melbourne, Australia). Sections of thickness 70 – 90nm were collected onto formvar-coated 100 mesh copper grids and stained sequentially with 1% uranyl acetate for 10 minutes and lead citrate for 5 minutes. The sections were imaged in a JEOL 1400+ transmission electron (JEOL Australasia, French Forest, NSW, Australia) microscope at 80kV, and images captured with a digital camera at a magnification of x3000 and x10,000 (Clive and Vera Ramaciotti Centre for Structural Cryo-Electron Microscopy, Monash University, Australia). Each section and electron micrograph were visualised in

a blinded manner for analysis purposes using Image J1.48 software (National Institutes of Health, Bethesda, Maryland, USA). Images at 2k resolution were used to determine glomerular basement membrane thickness. A minimum of three glomeruli from each kidney (n=3-4 mice/group) were examined. A total of 8-10 electron micrographs of nonoverlapping fields were taken from each glomerulus at a constant magnification of x2000. An average of 100 points per glomerulus was measured, after which the arithmetic mean ± SEM for glomerular basement membrane (GBM) thickness was determined for each mouse. The number of filtration slits was obtained by counting the number of slit pores per 100μm of GBM from each set of micrographs (x10,000).

Urinary 15-isoprostane F_{2t}

As a whole-body measure of oxidative stress, 15-Isoprostane F_{2t} was measured in urine by competitive ELISA (Oxford Biomedical Research, Oxford, UK).

Kidney fractionation

50mg of kidney cortex were homogenised using a Bullet blender (Next Advance, Lomb Scientific, Taren Point, NSW, Australia) with a cocktail of 1 and 2μm zirconium beads, in extraction buffer (20 mM HEPES buffer, pH7.2, 1 mM EGTA, 210 mM mannitol, 70 mM sucrose) to isolate nucleus, cytosol, mitochondria and plasma membrane as previously described.[S9, S10] Total protein was determined by the Bicinchoninic acid method (Pierce, Rockford, IL, USA).

Kidney RAGE protein expression

RAGE protein was determined in 1:200 diluted membrane extracts using a mouse RAGE DuoSet sandwich ELISA from R & D Systems (MRG00, Minneapolis, MN, USA). Absorbance was measured at 450nm on the Victor 3 plate reader (Perkin Elmer, Glen Waverley, Victoria, Australia).

Kidney Active TGF-β1 and Fibronectin

Biologically active TGF-β1 was measured in plasma membrane fractions using the TGF-β1 Emax ImmunoAssay System (Promega, Madison, WI, USA). Prior to measurement, samples were acid

activated with 1M HCl followed by neutralization to pH 7.0 with 1M NaOH. Values were expressed as pg/ml. Fibronectin was measured using a mouse Fibronectin ELISA kit according to the manufacturer's instructions (EK0351, Boster, Pleasanton, CA, USA).

Kidney NF-κB, MCP-1 and IL-10

Interleukin-10 (DY417-05, Mouse IL-10, DuoSet, R&D Systems, Minneapolis, USA) and MCP-1/CCL2 (DY479-05, Mouse MCP-1, DuoSet, R&D Systems, USA) in kidney cortex were measured by commercially available ELISA. NFκB DNA-binding activity was measured in nuclear isolates using the TransAM p65 NFκB DNA-binding activity assay (Active Motif, Carlsbad, CA).

Quantitative Real Time RT-PCR

RNA was isolated from renal cortex (20-30 mg) using TRIzol Reagent (Life Technologies). DNA-free RNA was reverse transcribed into cDNA using the Superscript First Strand Synthesis System according to the manufacturer's specifications (Life Technologies BRL, Grand Island, NY). Real-time qPCR was performed using TaqMan assays using a 7500 Fast Real-time PCR System (Applied Biosystem, VIC, Australia), and gene expression normalized relative to 18S ribosomal RNA. The relative fold difference in expression was calculated using the comparative 2-ΔΔCt method. Primers and probes were designed with Primer Express 2.0 software (Applied Biosystems). The probe and primer sequences for *Ager*, *Glp1r*, *Nlrp3*, *Il1b*, *Ccl2* (MCP-1), *Il10,* and *Txnip* appear in Table S1.

Single-Cell Sequencing

Preparation of kidney tissues was conducted at 4˚C with all buffers maintained on ice. Processed individually, each mouse kidney was collected and chilled in PBS before dissection of kidney cortex. The isolated cortex material was minced using a scalpel and pressed through a 100μM cell sieve using a 1 mL syringe plunger while rinsing material through with PBS. The resulting homogenate was collected in a 50 mL falcon tube and centrifuged at 250 x G for 2 minutes and the supernatant discarded. The pellet was

transferred to a 15 mL falcon tube using a Pasteur pipette with a volume of PBS up to 15 mL. The recovered fraction was centrifuged at 200 x G for 5 minutes, after which the supernatant was carefully removed to avoid disturbing pelleted material. The glomerular pellet was resuspended in 1 mL of digestion buffer (10 mg protease from bacillus licheniformis, 10uL DNase, 1uL 0.5 M EDTA, 1mL PBS), and allowed to digest for 13 minutes at 4˚ C with slow rotation. Further digestion was stopped by the addition of 1 mL of 20 % FBS in PBS. To aid dissociation, the mixture was additionally triturated using a 1000 µL pipette very gently. Triturated material was passed through a 40 µM cell sieve and collected in a 50 mL falcon tube by rinsing through with 2% FBS in PBS. Material that did not pass through the 40 µM sieve was further triturated until no remaining clumps remained on the sieve. Immediately prior to starting single cell capture, the dissociated glomerular fraction was centrifuged at 200 x G for 5 minutes, followed by repeated washes (at least 3 washes of 200 x G, 1 mL filtered PBS with 0.01% BSA, 2 minutes) to reduce free RNA in solution. Single-cell capture and transcriptome profiling were conducted using a droplet based technology "Drop-Seq" and a single-cell microfluidics platform designed by Dolomite-Bio according to "Drop-Seq Protocol version 3.1 Dec-2015"[S11] with minor modifications. Modifications include the use of Terra PCR Direct Polymerase Mix for cDNA amplification steps with 4 cycles in stage one and 11 cycles in stage two). Final sample libraries were created using the Nextera XT DNA Library Preparation Kit and sequenced using Illumina HiSeq in paired-end 150-cycle configuration by NovogeneAIT Genomics (Singapore).

Single-Cell sequencing Data Analysis

Raw single-cell reads were processed using Drop-Seq tools version 2.4[S12] including demultiplexing and retention of reads according to the top 3000 cell barcodes detected per sample, alignment of reads to mouse transcripts (GRCm38, Ensembl) and generation of transcript by cell count matrices

to be used in downstream analysis. Count matrices were imported into R as Seurat objects using the R package Seurat version 3.0.1.[S13] Subsequent quality filtering included removal of cells meeting any of the following criteria: cells having fewer than 400 or more than 3000 genes detected, cells with more than 20% of captured transcripts being mitochondrial. Quality filtered samples were normalised and integrated using Seurat functions NormalizeData and IntegrateData (dims=1:30) prior to clustering, which used PCA reduced dimensions (dims=1:23) for functions RunTSNE, FindNeighbors and FindClusters (res=0.8) to assign clusters. To identify cell types, cluster specific gene signatures were examined with Seurat's FindAllMarkers function and comparison with known endogenous marker gene expression. [S14, S15] Differential gene expression was calculated using the Seurat function FindMarkers specifying Wilcoxon rank sum analysis with min.pct set to 0.25. Cluster-wise differential gene expression was further assigned per gene ranking according to significance and fold change calculations as described previously[S16] for analysis of Reactome gene sets [S17] using the multi-contrast pathway enrichment tool 'mitch' (v1.0.8). [S18]

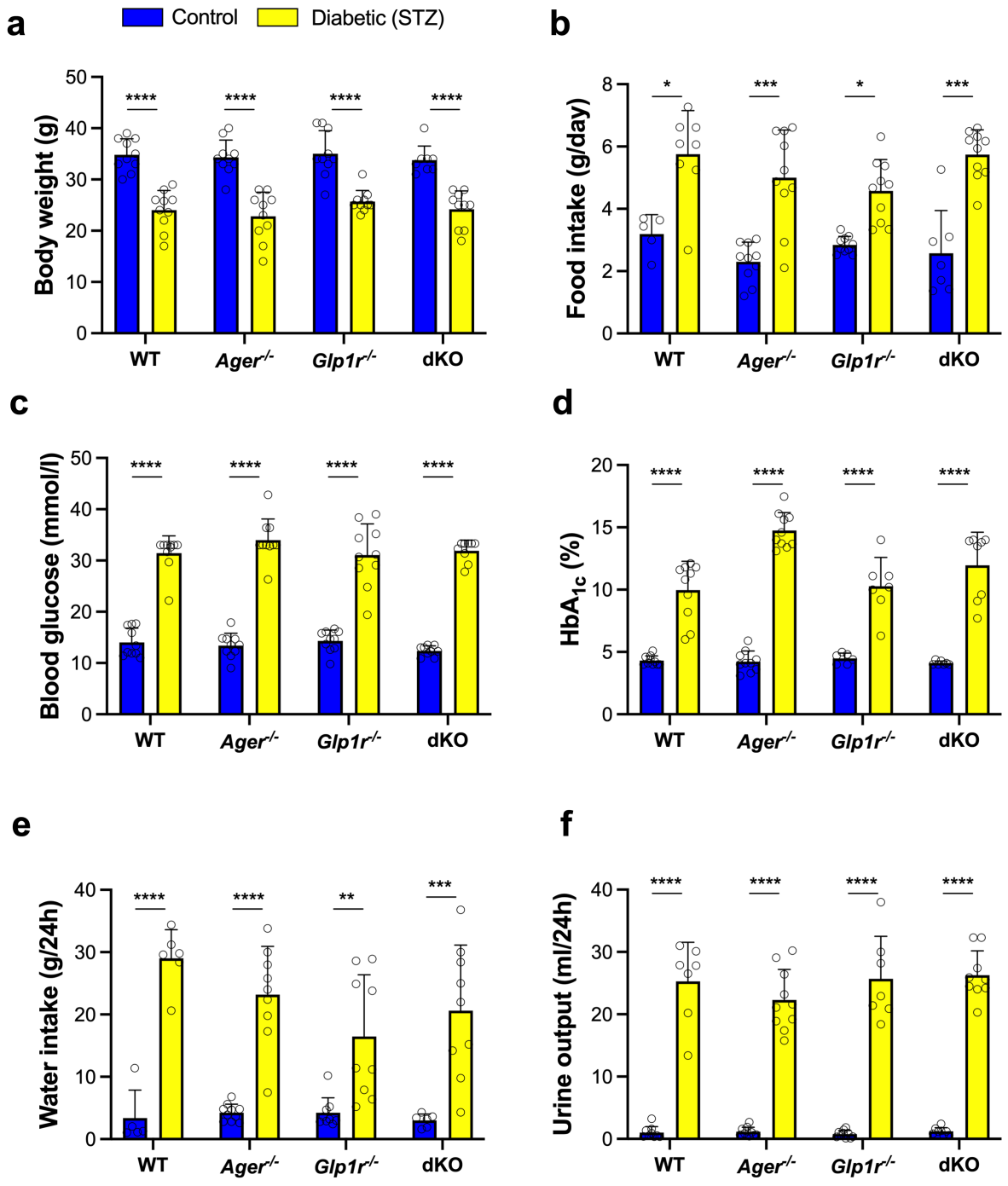

Fig. S1: No effect of genetic deletion of *Ager*, *Glp1r* or both *Ager* and *Glp1r in vivo* on physiological or metabolic features at study endpoint. WT, *ager-/-, glp1r-/-* and *ager-glp1r* dKO mice were rendered diabetic with STZ and followed for 24 weeks. **(a)** Body weight, **(b)** Food intake during 24h metabolic caging, **(c)** Blood glucose, **(d)** Glycated hemoglobin (HbA_{1c}), **(e)** Water intake during 24h metabolic caging, **(f)** Urine output during 24h metabolic caging. Data are displayed as mean ± SD. Dots represent individual mice. * $P<0.05$, ** $P<0.01$, *** $P<0.001$, **** $P<0.0001$. P values determined by two-way ANOVA with Tukey's multiple comparisons test. n=5-10 mice/group.

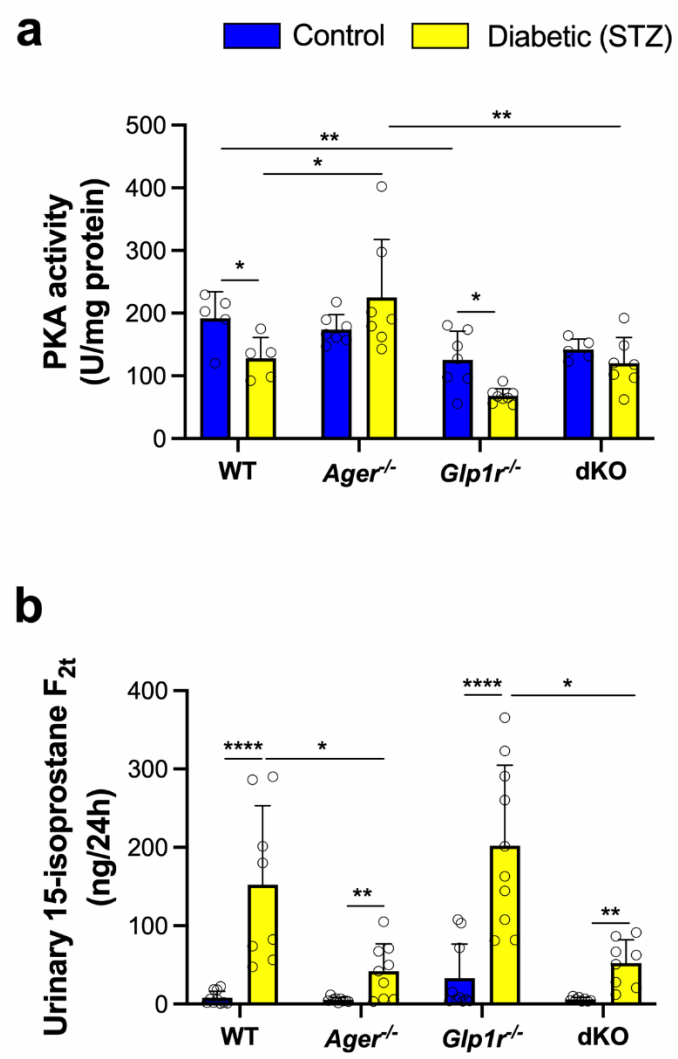

Fig. S2: Markers of GLP-1R activation and oxidative stress in *ager-/-*, *glp1r-/-* or *ager-glp1r* dKO mice. WT, *ager-/-*, *glp1r-/-* and *ager-glp1r* dKO mice were rendered diabetic with STZ and followed for 24 weeks. **(a)** PKA was determined in kidney cortex by ELISA. **(b)** 8-isoprostanes as determined by ELISA in 24 h urine collections. Data are displayed as mean ± SD. Dots represent individual mice. * $P<0.05$, ** $P<0.01$, **** $P<0.0001$. P values determined by two-way ANOVA with Tukey's multiple comparisons test. n=5-10 mice/group.

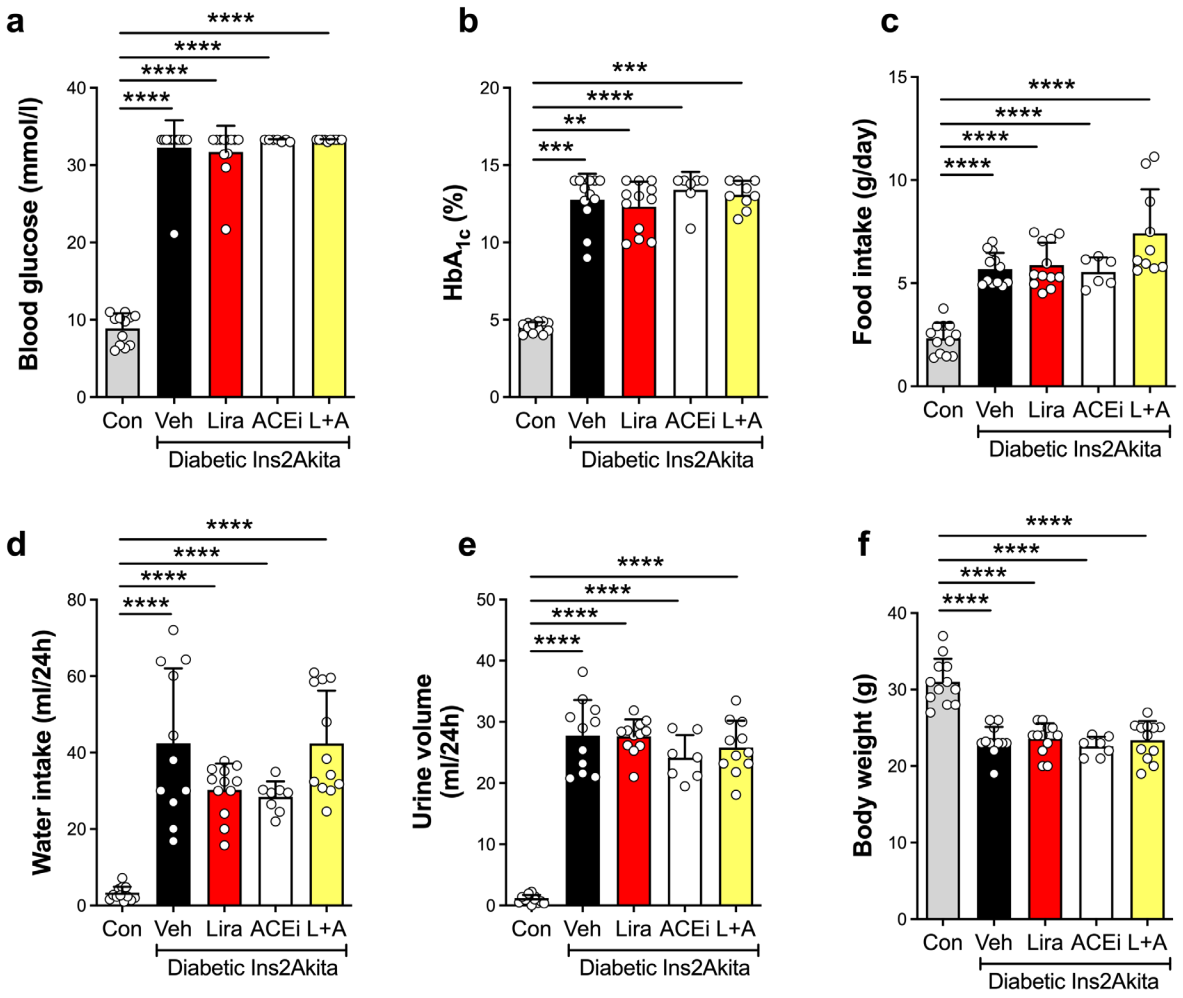

Fig. S3: No effect of pharmacological treatment with liraglutide, perindopril or combination therapy (liraglutide and perindopril) on physiological or metabolic features at study endpoint in Ins2Akita mice. **(a)** Blood glucose (glucometer), **(b)** Glycated hemoglobin (HbA_{1c}), **(c)** Food intake during 24h metabolic caging, **(d)** Water intake during 24h metabolic caging, **(e)** Urine output during 24h

metabolic caging, **(f)** Body weight. Data are displayed as mean ± SD. Dots represent individual mice. * $P<0.05$, ** $P<0.01$, *** $P<0.001$, **** $P<0.0001$. P values determined by two-way ANOVA with Tukey's multiple comparisons test. n=12 mice/group.

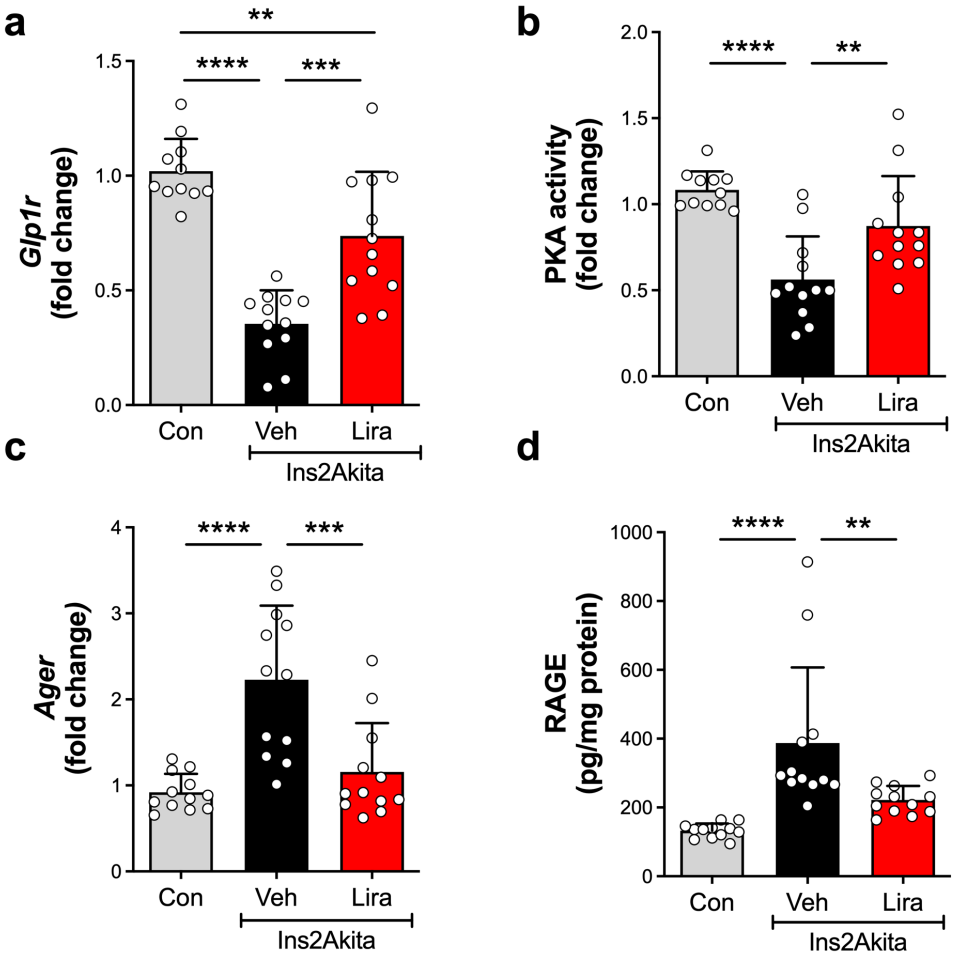

Fig. S4: Markers of GLP-1R activation and RAGE in kidney cortex in liraglutide-treated Ins2Akita mice. (a) *Glp1r* mRNA expression in kidney cortex. **(b)** PKA in in kidney cortex. **(c)** *Ager* mRNA expression in kidney cortex. **(d)** RAGE protein in kidney cortex. Data are displayed as mean ± SD. Dots represent individual mice. ** $P<0.01$, *** $P<0.001$, **** $P<0.0001$. P values determined by one-way ANOVA with Tukey's multiple comparisons test. n=11-12 mice/group.

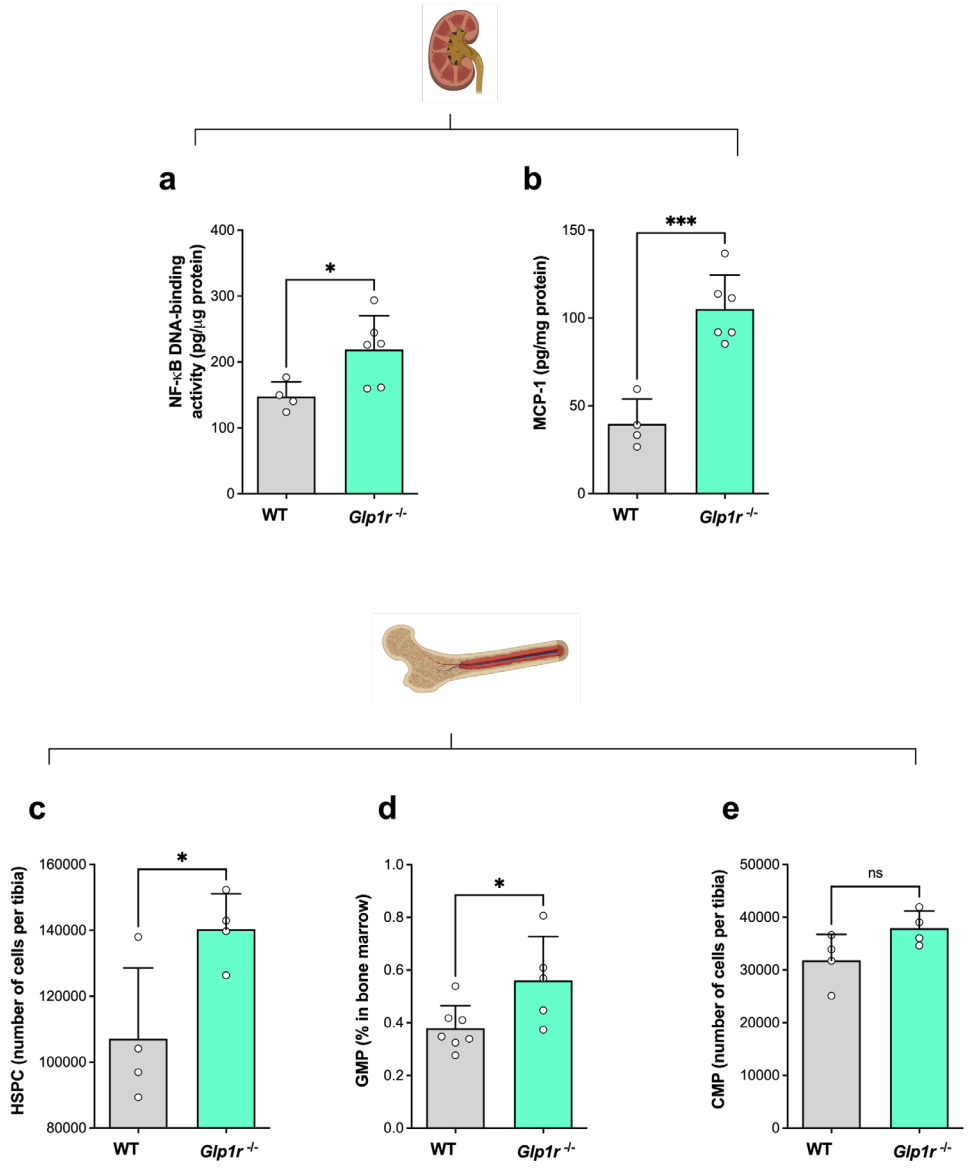

Fig. S5: Markers of inflammation in *Glp1r*-/- mice. **(a)** NF-κB DNA-binding activity in kidney cortex by ELISA. **(b)** Kidney MCP-1 protein by ELISA. **(c)** – **(e)** Bone marrow-derived progenitor cells were measured by flow cytometry: **(c)** HSPC, **(d)** GMP and **(e)** CMP. Data are mean ± SD (n=4-7/group). Dots represent individual mice. *P* values were determined by unpaired two-tailed t-test. * $P<0.05$, *** $P<0.001$.

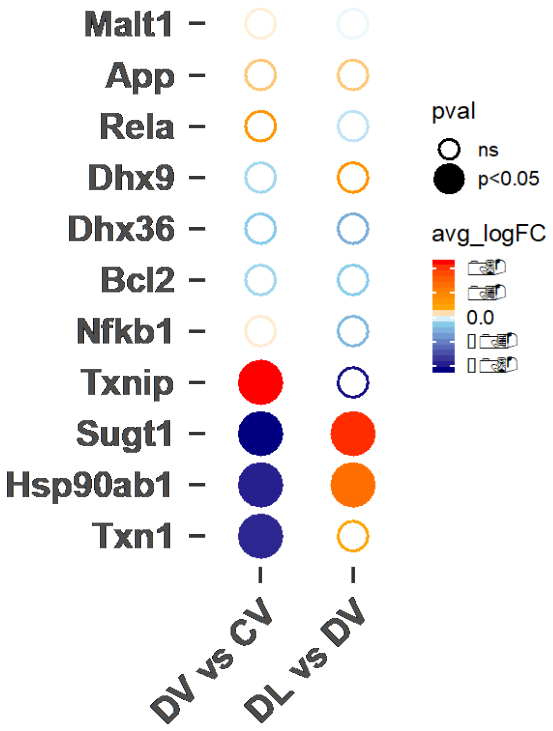

Fig. S6: Podocyte inflammatory signature.
Differential expression (average logFC) of detected inflammation set genes (Reactome) in podocytes from mice with diabetes versus control (Ins2-Akita DV vs Control CV) and diabetes versus diabetes plus liraglutide treatment (Ins2-Akita + Lira DL vs Ins2-Akita DV), n=4 mice per group.

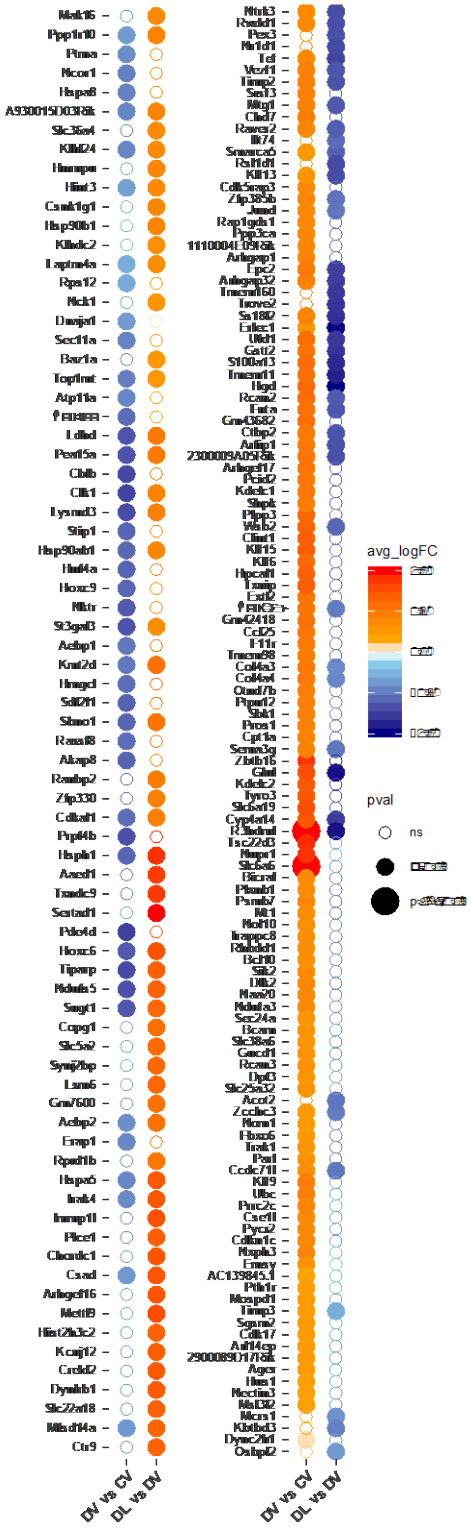

Fig. S7: Top 200 differentially expressed genes in the podocyte in response to liraglutide.
Top 200 differentially expressed genes in the podocyte cell population from single cell transcriptomic analysis in Ins2-Akita mice with or without liraglutide treatment. Right hand column follows on from left. DV, Ins2Akita Vehicle; DL, Diabetic liraglutide, n=4 mice per group. Differentially expressed genes between groups were determined using Seurat FindMarkers with Wilcoxon Rank Sum testing. *P*-value adjustment is based on Bonferroni correction using all genes in the dataset.

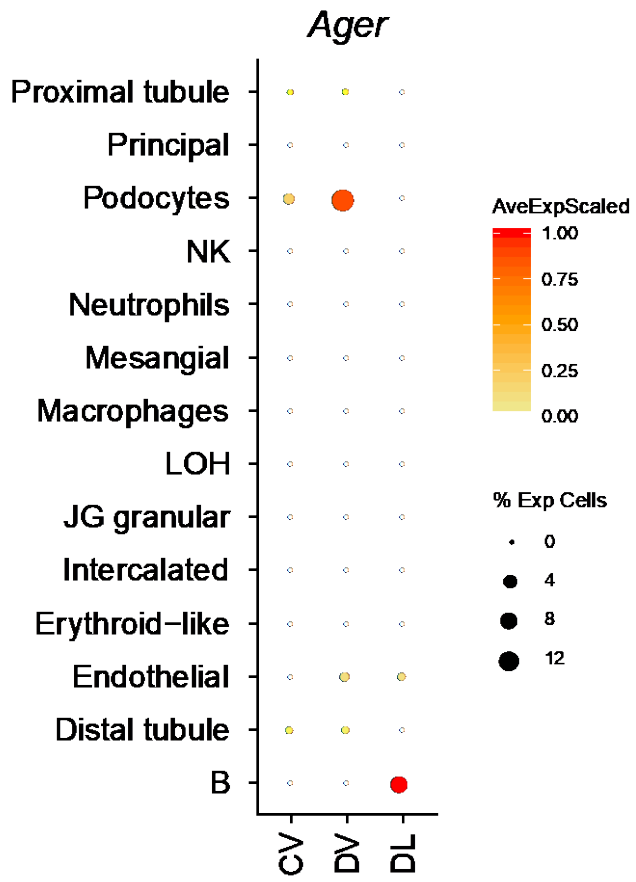

Fig. S8: Dot plot of *Ager* gene expression in Control versus Ins2-Akita mice with and without liraglutide treatment.

Ager expression in kidney cell populations from single cell transcriptomic analysis in in Control (CV), Ins2-Akita mice (DV) and Ins2-Akita mice treated with liraglutide (DL). Data are displayed as percentage cells expressing *Ager*. The average expression level is scaled, where 0 is not detected and 1 represents highest expression detected for *Ager*. n=4 mice per group.

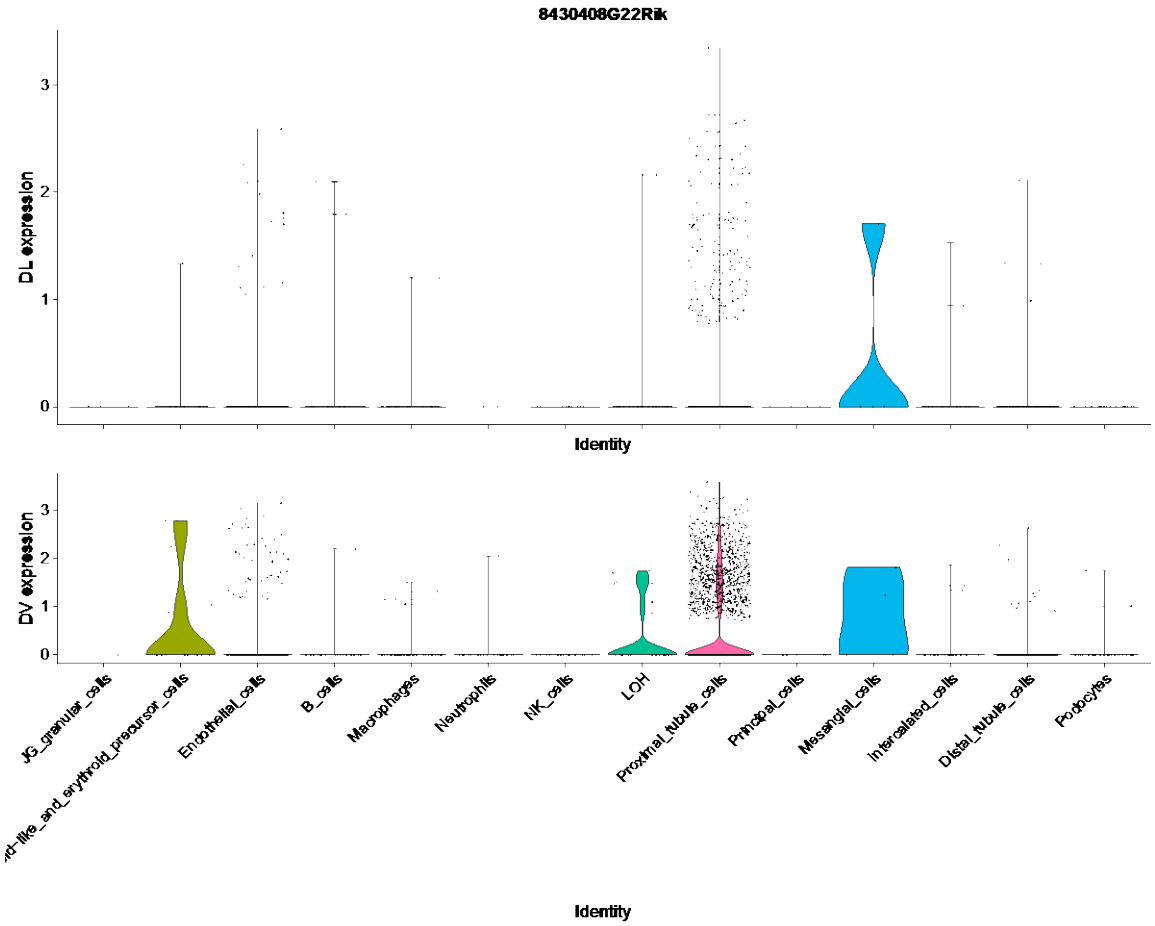

Fig. S9: Liraglutide reverses the *Depp1* gene signature in diabetes.

Depp1 expression in kidney cell populations from single cell transcriptomic analysis in Ins2-Akita mice with (top) or without (bottom) liraglutide treatment. DV, Ins2Akita Vehicle; DL, Diabetic liraglutide. Data are displayed as log2 normalised expression per cell per group, n=4 mice per group. Dots represent individual cells. Differentially expressed genes between groups were determined using Seurat FindMarkers with Wilcoxon Rank Sum testing. *P*-value adjustment is based on Bonferroni correction using all genes in the dataset.

Supplementary Table 1: Primer and Probe sequences for qRT-PCR

Target Gene	Forward Primer	Reverse Primer	Probe
Ager	GCTGTAGCTGGTGGTCAGAACA	CCCCTTACAGCTTAGCACAAGTG	6-FAM CACAGCCCGGATTG
Glp1r	TGGTGTTCCTGCTCATGCA	CCTTCCACCAGCAACCAGTAG	6-FAM CGTGGCAGCCAAC
Txnip	TTTTCAAGCCCTGACTTTAC	GGTTCAAGAAAAACGAAAGC	

Supplementary References

S1. Bierhaus A, Haslbeck KM, Humpert PM, *et al.* Loss of pain perception in diabetes is dependent on a receptor of the immunoglobulin superfamily. *J Clin Invest* 2004; **114:** 1741-1751.

S2. Constien R, Forde A, Liliensiek B, *et al.* Characterization of a novel EGFP reporter mouse to monitor Cre recombination as demonstrated by a Tie2 Cre mouse line. *Genesis* 2001; **30:** 36-44.

S3. Scrocchi LA, Brown TJ, MaClusky N, *et al.* Glucose intolerance but normal satiety in mice with a null mutation in the glucagon-like peptide 1 receptor gene. *Nat Med* 1996; **2:** 1254-1258.

S4. Tan SM, Ziemann M, Thallas-Bonke V, *et al.* Complement C5a Induces Renal Injury in Diabetic Kidney Disease by Disrupting Mitochondrial Metabolic Agility. *Diabetes* 2020; **69:** 83-98.

S5. Chen LH, Stead B, Advani SL, *et al.* Hyperglycemia and renal mass ablation synergistically augment albuminuria in the diabetic subtotally nephrectomized rat: implications for modeling diabetic nephropathy. *Nephron Extra* 2012; **2:** 115-124.

S6. Cummings BP, Stanhope KL, Graham JL, *et al.* Chronic administration of the glucagon-like peptide-1 analog, liraglutide, delays the onset of diabetes and lowers triglycerides in UCD-T2DM rats. *Diabetes* 2010; **59:** 2653-2661.

S7. Gilbert RE, Huang Q, Thai K, *et al.* Histone deacetylase inhibition attenuates diabetes-associated kidney growth: potential role for epigenetic modification of the epidermal growth factor receptor. *Kidney international* 2011; **79:** 1312-1321.

S8. Forbes JM, Thorpe SR, Thallas-Bonke V, *et al.* Modulation of soluble receptor for advanced glycation end products by angiotensin-converting enzyme-1 inhibition in diabetic nephropathy. *Journal of the American Society of Nephrology : JASN* 2005; **16:** 2363-2372.

S9. Coughlan MT, Thallas-Bonke V, Pete J, *et al.* Combination therapy with the advanced glycation end product cross-link breaker, alagebrium, and angiotensin converting enzyme inhibitors in diabetes: synergy or redundancy? *Endocrinology* 2007; **148:** 886-895.

S10. Thallas-Bonke V, Thorpe SR, Coughlan MT, *et al.* Inhibition of NADPH oxidase prevents advanced glycation end product-mediated damage in diabetic nephropathy through a protein kinase C-alpha-dependent pathway. *Diabetes* 2008; **57:** 460-469.

S11. Macosko EZ, Basu A, Satija R, *et al.* Highly Parallel Genome-wide Expression Profiling of Individual Cells Using Nanoliter Droplets. *Cell* 2015; **161:** 1202-1214.

S12. J. Nemesh and A. Wysoker. Drop-seq tools. *GitHub repository*.

S13. Butler A, Hoffman P, Smibert P*, et al.* Integrating single-cell transcriptomic data across different conditions, technologies, and species. *Nat Biotechnol* 2018; **36:** 411-420.

S14. Chung JJ, Goldstein L, Chen YJ*, et al.* Single-Cell Transcriptome Profiling of the Kidney Glomerulus Identifies Key Cell Types and Reactions to Injury. *Journal of the American Society of Nephrology : JASN* 2020; **31:** 2341-2354.

S15. Park J, Shrestha R, Qiu C*, et al.* Single-cell transcriptomics of the mouse kidney reveals potential cellular targets of kidney disease. *Science* 2018; **360:** 758-763.

S16. Rafehi H, Balcerczyk A, Lunke S*, et al.* Vascular histone deacetylation by pharmacological HDAC inhibition. *Genome Res* 2014; **24:** 1271-1284.

S17. Jassal B, Matthews L, Viteri G*, et al.* The reactome pathway knowledgebase. *Nucleic Acids Res* 2020; **48:** D498-D503.

S18. Kaspi A, Ziemann M. mitch: multi-contrast pathway enrichment for multi-omics and single-cell profiling data. *BMC Genomics* 2020; **21:** 447.